JOURNAL OF MAGNETIC RESONANCE IMAGING 34:729–749 (2011)

Review

Quantitative Assessment of Liver Fat with Magnetic Resonance Imaging and Spectroscopy

CME

Scott B. Reeder, MD, PhD,[1] Irene Cruite, MD,[2] Gavin Hamilton, PhD,[2] and Claude B. Sirlin, MD[2]*

This article is accredited as a journal-based CME acitivity. If you wish to receive credit for this activity, please refer to the website: www.wileyblackwellcme.com

ACCREDITATION AND DESIGNATION STATEMENT

Blackwell Futura Media Services designates this journal-based CME activity for a maximum of 1 *AMA PRA Category 1 Credit*™. Physicians should only claim credit commensurate with the extent of their participation in the activity.

Blackwell Futura Media Services is accredited by the Accreditation Council for Continuing Medical Education to provide continuing medical education for physicians.

EDUCATIONAL OBJECTIVES

Upon completion of this educational activity, participants will be better able to evaluate the effectiveness of current imaging techniques in assessing hepatic steatosis.

ACTIVITY DISCLOSURES

No commercial support has been accepted related to the development or publication of this activity.

Faculty Disclosures:

The following contributors have no conflicts of interest to disclose:

Editor-in-Chief: C. Leon Partain, MD, PhD

CME Editor: Scott B. Reeder, MD, PhD

CME Committee: Scott Nagle, MD, PhD, Pratik Mukherjee, MD, PhD, Shreyas Vasanawala, MD, PhD, Bonnie Joe, MD, PhD, Tim Leiner, MD, PhD, Sabine Weckbach, MD, Frank Korosec, PhD

Authors: Scott B. Reeder, MD, PhD, Irene Cruite, MD, Gavin Hamilton, PhD, Claude B. Sirlin, MD

This manuscript underwent peer review in line with the standards of editorial integrity and publication ethics maintained by *Journal of Magnetic Resonance Imaging*. The peer reviewers have no relevant financial relationships. The peer review process for *Journal of Magnetic Resonance Imaging* is double-blinded. As such, the identities of the reviewers are not disclosed in line with the standard accepted practices of medical journal peer review.

Conflicts of interest have been identified and resolved in accordance with Blackwell Futura Media Services's Policy on Activity Disclosure and Conflict of Interest. No relevant financial relationships exist for any individual in control of the content and therefore there were no conflicts to resolve.

INSTRUCTIONS ON RECEIVING CREDIT

For information on applicability and acceptance of CME credit for this activity, please consult your professional licensing board.

This activity is designed to be completed within an hour; physicians should claim only those credits that reflect the time actually spent in the activity. To successfully earn credit, participants must complete the activity during the valid credit period, which is up to two years from initial publication.

Follow these steps to earn credit:

- Log on to www.wileyblackwellcme.com
- Read the target audience, educational objectives, and activity disclosures.
- Read the article in print or online format.
- Reflect on the article.
- Access the CME Exam, and choose the best answer to each question.
- Complete the required evaluation component of the activity.

This activity will be available for CME credit for twelve months following its publication date. At that time, it will be reviewed and potentially updated and extended for an additional twelve months.

[1]Liver Imaging Research Program, Departments of Radiology, Medical Physics, Biomedical Engineering and Medicine, University of Wisconsin, Madison, Wisconsin USA.
[2]Liver Imaging Group, Department of Radiology, University of California San Diego, California USA.
Contract grant sponsor: National Institutes of Health (NIH); Contract grant numbers: R01-DK083380, R01-DK088925, RC1-EB010384-01; Contract grant sponsors: Coulter Foundation; University of Wisconsin IEDR; GE Healthcare.
*Address reprint requests to: C.B.S., Liver Imaging Group, Department of Radiology, University of California, San Diego, 408 Dickinson Street, San Diego, CA 92103-8226. E-mail: csirlin@ucsd.edu
Received November 7, 2010; Accepted February 24, 2011.
DOI 10.1002/jmri.22580
View this article online at wileyonlinelibrary.com.

Hepatic steatosis is characterized by abnormal and excessive accumulation of lipids within hepatocytes. It is an important feature of diffuse liver disease, and the histological hallmark of nonalcoholic fatty liver disease (NAFLD). Other conditions associated with steatosis include alcoholic liver disease, viral hepatitis, human immunodeficiency virus (HIV) and genetic lipodystrophies, cystic fibrosis liver disease, and hepatotoxicity from various therapeutic agents. Liver biopsy, the current clinical gold standard for assessment of liver fat, is invasive and has sampling errors, and is not optimal for screening, monitoring, clinical decision-making, or well suited for many types of research studies. Noninvasive methods that accurately and objectively quantify liver fat are needed. Ultrasound (US) and computed tomography (CT) can be used to assess liver fat but have limited accuracy as well as other limitations. Magnetic resonance (MR) techniques can decompose the liver signal into its fat and water signal components and therefore assess liver fat more directly than CT or US. Most MR techniques measure the signal fat-fraction (the fraction of the liver MR signal attributable to liver fat), which may be confounded by numerous technical and biological factors and may not reliably reflect fat content. By addressing the factors that confound the signal fat-fraction, advanced MR techniques measure the proton density fat-fraction (the fraction of the liver proton density attributable to liver fat), which is a fundamental tissue property and a direct measure of liver fat content. These advanced techniques show promise for accurate fat quantification and are likely to be commercially available soon.

Key Words: hepatic steatosis; fat quantification; magnetic resonance imaging; magnetic resonance spectroscopy; magnitude; complex; fat-fraction
J. Magn. Reson. Imaging 2011; 34:729–749.

HEPATIC STEATOSIS is a common condition of the liver, characterized by accumulation of lipid within hepatocytes. It is the histological hallmark of nonalcoholic fatty liver disease (NAFLD) but also may occur with alcoholic liver disease, viral hepatitis, cystic fibrosis liver disease, and human immunodeficiency virus (HIV) and genetic lipodystrophies, as well as a manifestation of drug toxicity. This article first describes the clinical features of hepatic steatosis and current methods for its diagnosis. Imaging techniques that assess steatosis are then discussed, including ultrasound (US), computed tomography (CT), and magnetic resonance (MR) techniques. MR techniques are classified into those that measure the signal fat-fraction and those that address known confounding factors, allowing measurement of the proton density fat-fraction.

HEPATIC STEATOSIS: OVERVIEW

Clinical Features

Hepatic steatosis is the abnormal and excessive accumulation of lipid vacuoles within hepatocytes, primarily as triglycerides, although other lipid metabolites such as free fatty acids, cholesterol, and phospholipids may also be present. It affects over 20% of the general population and is associated with disorders that result in diffuse liver fat deposition, such as NAFLD, hepatitis, drug toxicities, alcoholic liver disease, lipodystrophy, parenteral nutrition, and pregnancy. Historically thought of as an incidental consequence of such disorders, hepatic steatosis is now increasingly recognized as a key pathogenic process and meaningful pathological feature of many hepatic and systemic disorders (1–11).

NAFLD, present in 20–80 million Americans, is the most common chronic liver disease in the United States (12–14). Hepatic steatosis is the histological hallmark of NAFLD and is accepted by most investigators to play a pathogenic role in the development of nonalcoholic steatohepatitis (NASH), a more aggressive subset of NAFLD, characterized by necroinflammation, fibrosis, and, eventually, cirrhosis (8,15–17). Free fatty acids, the substrate for triglyceride formation, trigger cell death by inducing oxidative stress, provoking production of cytokines and reactive oxygen species, which activates apoptosis, resulting in NAFLD progression. Five to 15% of patients with NAFLD present with established cirrhosis on liver biopsy (8,16,17), while 4%–5% of individuals with isolated steatosis eventually develop cirrhosis (8,11). In patients who have progressed to NAFLD-related cirrhosis, about 7% will develop hepatocellular carcinoma (HCC) over a 10-year timeframe (10). Hepatic steatosis may even have direct carcinogenic effects, as HCC has been described in patients with NAFLD without fibrosis or cirrhosis (18), although the relative contribution of steatosis and necroinflammatory activity to hepatocarcinogenesis in such patients has not been delineated.

In addition to contributing to liver injury, hepatic steatosis also has systemic implications. Steatosis interferes with insulin signaling, contributes to hepatic insulin resistance, and may be the pathogenic link between obesity and its metabolic complications (3,4). Hepatic steatosis is an established risk factor for, and may even contribute to, the development of diabetes; in longitudinal studies, 20%–50% of individuals with steatosis subsequently develop diabetes (2,11). Emerging data also shows hepatic steatosis to be an independent risk factor for cardiovascular mortality (19) beginning in the fifth decade of life (3), with cardiovascular disease being the most common cause of morbidity and mortality in patients with NAFLD (3,9,19,20).

While the importance of hepatic steatosis is most obvious in NAFLD, steatosis is also relevant in other conditions. Concomitant occurrence of steatosis and viral hepatitis (especially certain hepatitis C virus genotypes) often heralds a worse prognosis with accelerated progression to cirrhosis. Steatosis may also affect the efficacy of antiviral therapy (6,7) in such patients. In patients undergoing liver surgery, hepatic steatosis reduces hepatocellular functional reserve and contributes to postoperative hepatic failure (21–23).

Diagnosis

Accurate, quantitative biomarkers of hepatic steatosis are necessary for accurate detection of steatosis,

grading of the disease severity, clinical decision-making, prognosis, and longitudinal monitoring of therapy. Qualitative biomarkers are insufficient for accurate detection, which requires a quantitative threshold to classify fat content as below or above a pathologic threshold. The relevant classification threshold also depends on the clinical context and may vary widely, from the standard 5% steatosis threshold often used for defining hepatic steatosis, to the 30% threshold for exclusion of liver transplantation donors (24).

Currently, liver biopsy is considered the gold standard for diagnosing and grading hepatic steatosis. At biopsy, hepatic steatosis is graded on a scale of 0–3 through subjective visual estimation of the proportion of hepatocytes containing intracellular vacuoles of fat. Steatosis grades are categorized into broad brackets of severity: grade 0 (normal) = up to 5% of cells affected, grade 1 (mild) = 5%–33% of cells affected, grade 2 (moderate) = 34%–66% of cells affected, and grade 3 (severe) = ≥67% of cells affected (25). Because these grading estimations are subjective, there is considerable inter- and intraindividual variation in steatosis grading at histopathology. Objective measurement of steatosis using computer image analysis of histology slides is possible (26,27) but is not done routinely in clinical practice. Regardless of whether steatosis is graded subjectively by visual estimation or objectively by computer image analysis, assessment of steatosis on histology slides fundamentally is a 2D measurement. As such, it may not reliably reflect fat content in 3D liver parenchyma.

As we describe below, all MR-based techniques assess liver fat in 3D tissue voxels; thus, while histology is the accepted clinical gold standard for diagnosis and grading of steatosis, it is probably not a well-suited reference standard for assessing the accuracy of the MR-based fat content measurement techniques, described later in this article. A more suitable reference standard is liver tissue triglyceride concentration, by definition a 3D metric of hepatic fat content. Liver tissue triglyceride concentration can be measured via biochemical assay, but this is a destructive procedure. Tissue submitted for biochemical assay cannot be submitted for histological analysis, and important features other than fat content (eg, necroinflammatory activity, fibrosis, iron) cannot be assessed. For this reason, biochemically determined liver tissue triglyceride concentration is not routinely measured.

Whether biopsy specimens are analyzed histologically or biochemically, biopsy is an invasive procedure with inherent risks, and it is expensive relative to imaging methods. It carries a small but not negligible risk of hospitalization (1%–3%) and even death (1:10,000) (28). It also entails several hours of post-procedure recovery requiring a missed work or school day for both the patient and a caretaker. Furthermore, biopsy is subject to sampling variability, as it evaluates only a small portion (0.05 cm^3) of the liver (800–1000 cm^3) (29–38), and the distribution of fat throughout the liver may be nonuniform. Although it is unknown whether such sampling variability cause errors in diagnosis, it may lead to important errors during longitudinal assessment of liver fat. For these reasons, a noninvasive, safe, and accurate method for detection and quantification of hepatic steatosis without sampling variability is necessary. As we describe below, US and CT can be used to assess steatosis but have important limitations, while MR-based techniques, particularly new techniques that measure the proton density fat-fraction, have the potential to meet this clinical and research need.

Why Quantitative Biomarkers for NAFLD With MRI?

In general, a quantitative biomarker is necessary for both accurate detection of disease (ie, make the correct diagnosis) and for accurate grading of disease severity (ie, quantification). Accurate diagnosis is necessary before therapy can be initiated, and accurate quantification is needed to determine prognosis and guide therapy.

Quantitative biomarkers can be used for disease diagnosis and clinical decision making by applying "sliding scale" cutoff values for binary classification of disease presence or absence (eg, fatty liver vs. normal) or disease severity (eg, disease sufficiently severe to warrant intervention vs. disease sufficiently mild to warrant observation only). The appropriate cutoff value often depends on the specific application. For example, a low cutoff value is likely to be appropriate for screening for early fatty liver disease (which requires high sensitivity to borderline abnormal elevations in liver fat content), whereas a higher cutoff value is likely to be appropriate for therapy initiation and selection (eg, exercise vs. drugs vs. bariatric surgery vs. observation only), and a different cutoff value may be appropriate for other indications such as selection of potential living-related liver transplant donors.

Unfortunately, there are not yet clinically defined cutoff values for normal vs. abnormal levels of hepatic fat or for levels that warrant different forms of therapy. A large MR spectroscopy study performed by Szczepaniak et al (14) in 2349 participants of the Dallas Heart Study defined a 95th percentile cutoff of 5.56% fat-fraction as abnormal, based on a subset of 345 patients with no identifiable risk factors for hepatic steatosis. This landmark study provides initial guidance for an appropriate cutoff value for detection of fatty liver, although future studies relating the fat-fraction to histology or to clinical outcome may modify this cutoff value slightly.

Regardless, as the current fat-fraction cutoff value for detection of fatty liver is low (on the order of 5%), the accuracy (bias) and precision (standard deviation) of a quantitative fat content biomarker must be far smaller than 5%–6% to provide reliable diagnosis. The exact accuracy and precision needed for a clinically useful biomarker of liver fat content is uncertain and remains to be determined. Clearly, the more accurate and precise a biomarker is, the better, particularly when early detection is important and subtle changes during therapy are meaningful. In addition, accurate and precise biomarkers are especially valuable in clinical trials, in order to reduce the number of subjects

needed to demonstrate efficacy of a treatment with statistical significance.

ULTRASOUND ASSESSMENT OF HEPATIC STEATOSIS

US is the most common imaging modality used to evaluate hepatic steatosis (39–41) because of its low cost, safety, and availability. It evaluates liver fat content indirectly based on subjective qualitative sonographic features such as liver echogenicity, echotexture, vessel visibility, and beam attenuation. Because it is operator- and machine-dependent, US has limited repeatability and reproducibility. It is also challenging to perform in obese patients (42) due to impaired beam penetration and limited liver visualization. Its positive predictive value for detection of steatosis is only 62%–77% (41,43). Utility of US in objective quantification of steatosis is hampered by factors such as fibrosis, edema, and extrahepatic adipose tissue. These factors confound the analysis of beam attenuation and echotexture, leading to unavoidable errors in fat quantification. US should thus be avoided, if possible, if there is need for early detection of steatosis, or if precise and accurate assessment of hepatic steatosis is needed. If US is performed, the results should be interpreted cautiously.

COMPUTED TOMOGRAPHY ASSESSMENT OF HEPATIC STEATOSIS

Unenhanced CT is a widely used imaging modality that evaluates hepatic steatosis indirectly based on hepatic x-ray attenuation. Unlike the US features mentioned above, x-ray attenuation can be measured objectively and with high precision (41,44–46). However, several factors other than fat (eg, presence of iron, copper, glycogen, fibrosis, and edema; ingestion of drugs such as amiodarone and gold) affect CT attenuation values, resulting in unavoidable errors in fat quantification (46) and low sensitivity for mild–moderate steatosis. Moreover, because CT relies on ionizing radiation, it is not suitable for use in children (47), or for longitudinal monitoring of adults with liver fat. Finally, inherent variability in attenuation values across CT scanners that manufactured by different vendors often results in different attenuation values (48). This variability can lead to a platform-dependent measurement of fat content with CT and is an important limitation of CT for liver fat quantification.

MR ASSESSMENT OF HEPATIC STEATOSIS

Overview

The two noninvasive MR-based techniques used for assessment of hepatic steatosis are MR spectroscopy (MRS) and MRI. The two techniques have the same underlying MR physics concepts, and they both exploit the difference in resonance frequencies between water and fat proton signals to quantitatively measure the signal fat-fraction and/or the proton density fat-fraction. Signal fat-fraction refers to liver signal attributable to fat, while proton density fat-fraction refers to the fraction of mobile protons in liver attributable to fat.

To calculate the signal or proton density fat-fraction using MRS or MRI, liver signal is first decomposed or separated into its fat and water signal components using a suitable MR-based water-fat separation technique. Several water-fat separation techniques can be used, and each decomposes the liver signal in a different manner, as discussed in subsequent sections. A key concept is that MR techniques are unique in their ability to decompose the liver signal into its water and fat components, and hence assess hepatic steatosis more directly than US or CT.

After the liver signal is decomposed, the signal fat-fraction (η) is calculated as the signal from fat protons divided by the combined signal from fat and water protons in the liver, ie:

$$\eta = \frac{F}{W + F} \quad [1]$$

An important property of the signal fat-fraction is that it is independent of the sensitivity of radiofrequency (RF) coils ("B_1" sensitivity). Calculating a fraction from spatially colocalized water and fat signals provides normalization that removes the influence of coil sensitivity, thereby avoiding errors introduced by inhomogeneous coil sensitivity when muscle or spleen is used as an internal calibration or normalization measurement. Signal fat-fraction generated with the MRS or MRI methods described below are, therefore, independent of signal variation due to B_1 coil sensitivities across the body. As we describe later in this article, signal fat-fraction can be calculated at the level of an MRS voxel or, in the case of imaging, pixel-by-pixel to form a signal fat-fraction parametric "map."

Because numerous biological, physical, and technical factors influence the relative MR signals from fat and water, however, the signal fat-fraction is a confounded measure of steatosis, does *not* reliably reflect the fat content within the liver, and is not a consistently reliable or standardized biomarker of hepatic steatosis. Importantly, confounding factors lead to measures of fat content that are platform and imaging protocol-dependent—different scanners or different scan parameters may yield meaningfully different apparent signal fat-fractions. This behavior renders signal fat-fraction impractical as a biomarker of liver fat.

To convert the confounded signal fat-fraction into an unconfounded proton density fat-fraction, the effects of all confounding factors must be addressed. The specific confounding factors depend on the technique used and may include T1 bias, T2 relaxation, T2* decay, spectral complexity of the fat spectrum, J-coupling, noise bias, and eddy currents. These factors are discussed in detail below in the section "MR Techniques That Measure Proton Density Fat-Fraction."

After minimizing or correcting all confounding factors, the signal fat-fraction is equivalent to the proton density fat-fraction. Measured correctly, the proton density fat-fraction is unconfounded by the biological, physical, and technical factors that confound the

signal fat-fraction; is independent of field strength, scanner platform, and specific scanning parameters; and correlates highly with biochemically determined liver tissue triglyceride concentration. Thus, unlike the signal fat-fraction, the proton density fat-fraction reflects the content of fat in the liver and potentially is a reliable, meaningful, and standardized biomarker of hepatic steatosis. Indeed, the proton density fat-fraction represents a fundamental measure of fat content, and its platform and scan parameter independence is a characteristic strength as a useful biomarker.

In the sections below we describe in more detail techniques that measure the signal fat-fraction and the proton density fat-fraction. The discussion begins with techniques that measure the signal fat-fraction, because these are the foundation upon which more advanced techniques have been developed to measure the proton density fat-fraction.

MR Techniques That Measure the Signal Fat-Fraction

MRS

MRS is the most direct MR-based method to separate the liver signal into its water and fat components and calculate a signal fat-fraction. MRS depicts proton signals as a function of their resonance frequency (Fig. 1). The resonance frequencies corresponding to protons in water and to the dominant protons in fat are distinct, can be identified based on prior knowledge, and can be quantified directly from the spectral tracing. Once the signal intensities at frequencies corresponding to water and fat are quantified, the signal fat-fraction is calculated using Eq. 1.

Collection of spectra for signal fat-fraction estimation requires proper acquisition technique. Typically a single voxel (typically $2 \times 2 \times 2$ cm^3 or $3 \times 3 \times 3$ cm^3) is manually placed in liver parenchyma, using multiplanar localizing images to avoid liver edges, large vessels, and large bile ducts. Shimming is then performed to achieve a homogeneous magnetic field across the voxel. After successful shimming a spectroscopic sequence is performed. One of two spectroscopic sequences are typically used: stimulated echo acquisition mode (STEAM) and point-resolved spectroscopy (PRESS). Both sequences are suitable for estimation of the signal fat-fraction. The STEAM consists of three 90° pulses and is capable of shorter TEs (as there is no TE evolution between the second and third RF pulses) than PRESS (90°–180°–180°). However, the use of stimulated echo in STEAM results in the signal-to-noise-ratio (SNR) of STEAM being half that of PRESS. As we will discuss later, however, STEAM is probably more appropriate for estimation of the proton density fat-fraction.

In performing single-voxel spectroscopy to estimate the liver fat-fraction, neither water nor fat saturation should be employed, as the signal intensities from both species are necessary to make the calculation. In addition, spatial saturation bands should not be used because saturation bands may partially saturate the signals arising from the voxel, and the degree to which water and fat signals are saturated may be unequal, leading to errors in the proportion of the liver signal attributed to fat. Although many authors advocate spectroscopic acquisition using many averages during free breathing, we find this to be unnecessary for assessment of fractional liver fat content, as the signal from even minimal amounts of liver fat can be readily detected and quantified without high SNR. For this reason and to save time, we prefer to collect spectra during a single breath-hold.

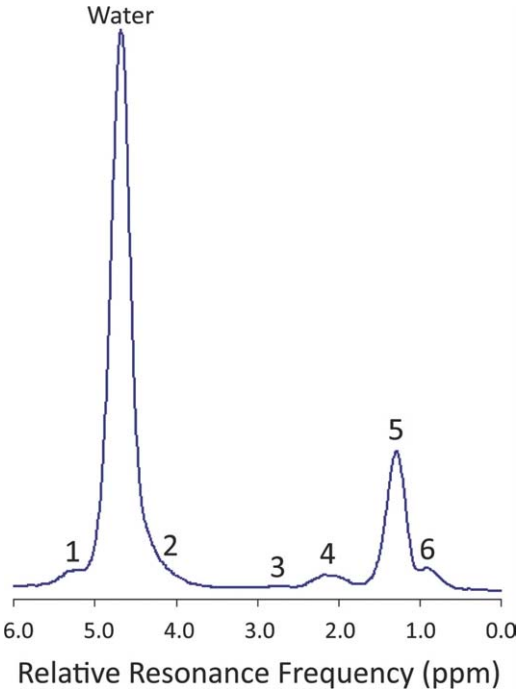

Figure 1. Fatty liver spectrum in a 44-year-old woman with fatty liver disease. An MR spectrum was acquired from a single $20 \times 20 \times 20$ mm^3 voxel in the right lobe during a single breath-hold without averaging using the STEAM sequence at 3T (TR/TE = 3500/10 msec; mixing time = 5 msec). Six distinct fat peaks can be resolved in vivo at clinical field strengths, as labeled (1–6), corresponding to the peaks in Table 1.

The analysis of collected spectra requires expertise and, currently, must be performed offline with specialized software. Automated, reliable, online analysis methods are not yet available, although are under development and may be commercially available in the near future. A full description of the analysis is beyond the scope of this review article, but key concepts are highlighted below.

The water spectrum is simple, as the two hydrogen protons in a water molecule have the same chemical environment, experience an identical magnetic field, and resonate at the same frequency. Consequently, the water spectrum consists of a single resonance peak. By convention, the center frequency of this peak is described in parts per million (ppm) with respect to a reference proton moiety (tetramethylsilane), which arbitrarily is assigned a relative resonance frequency of 0 ppm. The frequency (or chemical shift) of water protons relative to the reference proton

Table 1
Proton MR Spectrum of Liver Triglycerides

Peak	In vivo ppm	Ex vivo ppm	Chemical environment	Type	Relative magnitude
1	5.3	5.29	-C**H** =C**H**-	Olefinic	4.7%
		5.19	-C**H**-O-CO-	Glycerol	
Water	4.7	4.70	$\mathbf{H}_2O$	—	—
2	4.2	4.20	-C$\mathbf{H}_2$-O-CO-	Glycerol	3.9%
3	2.75	2.75	-CH=CH-C$\mathbf{H}_2$-CH=CH-	Diacyl	0.6%
4	2.1	2.24	-CO-C$\mathbf{H}_2$-CH_2-	α-Carboxyl	12.0%
		2.02	-C$\mathbf{H}_2$-CH=CH-C$\mathbf{H}_2$-	α-Olefinic	
5	1.3	1.60	-CO-CH_2-C$\mathbf{H}_2$-	β-Carboxyl	0.7
		1.30	-(C$\mathbf{H}_2$)$_n$-	Methylene	
6	0.9	0.9	-$(CH_2)_n$-C$\mathbf{H}_3$	Methyl	0.088

Proton MR spectrum of liver fat measured by Hamilton et al (84). The different liver fat proton moieties (bold H) produce nine resonances ex vivo at high field strength. In vivo, at clinical field strengths, these resonances are resolvable into six distinct fat peaks, though peaks 1 and 2 cannot be clearly distinguished from water. The liver spectrum can be used to correct for fat peaks included in water in MRS, as well as spectral modeling used in advanced imaging techniques (60,63,78,82,95). The relative magnitudes listed may not apply to other fat depots.

depends on temperature; at 37°C it is 4.70 ppm. By comparison, the fat proton spectrum is complicated, as the multiple hydrogen protons in fat have different chemical environments, experience nonidentical magnetic fields, and resonate at different frequencies. A typical fat molecule has nine chemically distinct proton moieties, each with a unique resonance frequency. While spectral peaks corresponding to each moiety are discernible in high-resolution spectroscopy performed in fat samples at high field strength, there is insufficient spectral resolution at clinical field strengths (eg, 1.5T or 3T) to delineate each peak, and some of the peaks blend together, forming six well-defined peaks at clinical field strengths (Table 1). As discussed in more detail later, two of the peaks have similar frequencies as water and, in spectra acquired from fatty livers, are superimposed with and obscured by the larger liver water peak (Fig. 1).

Once the visible peaks are identified the area under each peak is quantified, usually by modeling each peak as a Gaussian distribution or a set of overlapping Gaussian distributions. The fat signal then is calculated as the sum of the area of the fat peaks (2.1, 1.3, and 0.9 ppm) or as the area of the main CH_2 peak (1.3 ppm). The signal fat-fraction can then be given as the fat signal divided by the sum of the water and fat peaks areas. Importantly, the signal fat-fraction with MRS has a dynamic range of 0%–100%.

Virtually all spectroscopy in the liver is limited to single-voxel acquisition. While multivoxel spectroscopy permits coverage of larger volumes in the liver, its inherent problems have limited its application. The large volume reduces the quality of the shim and hence the quality of the spectra. The time required for multivoxel spectroscopy lies well beyond the range of single breath-hold techniques, leading to breathing-induced artifacts.

MRI

MRI-based techniques that measure the signal fat-fraction have been used for over 25 years (49). These include fat-suppressed techniques and chemical shift-based techniques.

Fat-Suppressed Techniques. Fat-suppressed techniques separate the liver MR signal into its fat and water components by comparing magnitude images acquired with and without chemical fat saturation (or selective water excitation). Fat-saturation (or selective water-excitation) pulses are used to suppress fat signal, which decreases the overall liver signal in a fat-containing liver. This effect is seen with either T1-weighted or T2-weighted sequences. Two sets of images, one with and the other without fat suppression, are acquired with identical imaging parameters, and comparison made to each other for fat assessment. In the presence of fat, the signal is higher on the nonfat-suppressed images than on the fat-suppressed images (Fig. 2), and the difference in signal intensity is entirely attributed to the presence of fat. Thus, the signal intensity from nonfat-suppressed images is assumed to represent the sum of water and fat signals (W + F), the signal intensity from fat-suppressed images is assumed to represent water signal (W), and the difference in signal intensity between nonfat-suppressed and fat-suppressed images is assumed to represent the fat signal (F). After making these assumptions, the signal fat-fraction (η) can be calculated as:

$$\eta = \frac{(S_{NFS} - S_{FS})}{S_{NFS}} \quad [2]$$

where S_{NFS} and S_{FS} are the signal intensities of liver without and with fat suppression, respectively.

Assuming perfect fat suppression, the equation above is valid, and this method estimates the signal fat-fraction with a dynamic range of 0%–100%. In one retrospective study, better correlation was shown between signal loss in fat-suppressed T2 weighted FSE imaging and biopsy steatosis grade than with dual echo imaging (50). A potential problem with fat-suppressed techniques is that the complete and homogeneous suppression of the fat signal by the chemical fat saturation (or selective water excitation) pulse is difficult if not impossible to reliably achieve throughout the liver (Fig. 2), due to inhomogeneous main magnetic field (B_0). This may result in incomplete fat suppression or even

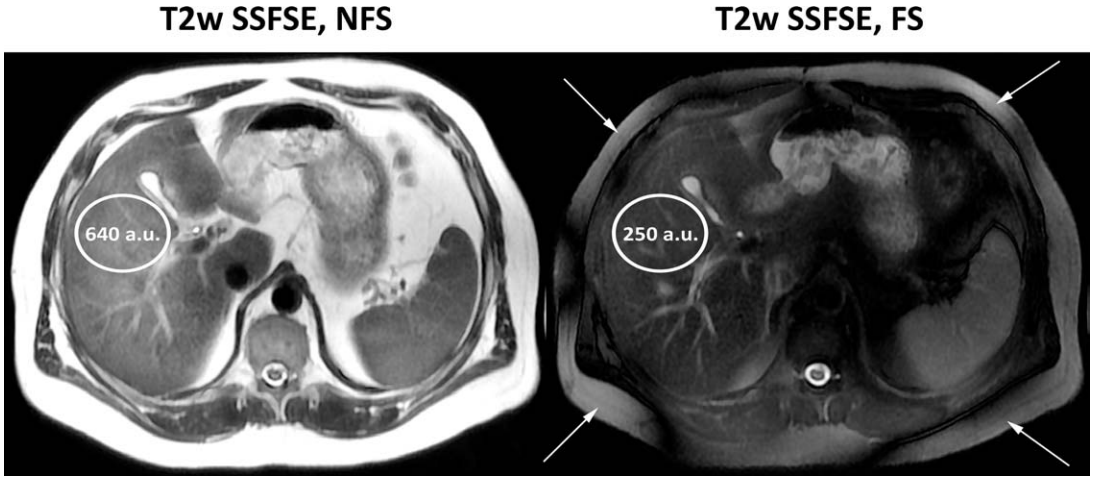

Figure 2. Signal fat-fraction using fat-suppressed MRI technique, acquired in a 32-year-old man with fatty liver disease. Axial T2-weighted single shot fast spin echo images of the liver acquired with no fat saturation (NFS, left) and with fat saturation (FS, right). The signal in a colocalized region of interest (oval) is 640 arbitrary units (a.u.) in the NFS image and 250 a.u. in the FS image. Using Eq. [2], the calculated signal fat-fraction is (640-250)/640 = 61%. The true fat-fraction by MR spectroscopy (not shown) is 17%, illustrating that the fat-suppressed MRI techniques may produce erroneous estimates of hepatic fat-content. Incomplete fat saturation and inadvertent water suppression (arrows) are potential pitfalls with fat-suppressed MRI techniques.

inadvertent water suppression, and Eq. 2 may not be entirely valid. While the fat saturation technique is suitable for estimation of the signal fat-fraction, it has not been widely researched as a method to measure proton density fat-fraction, and will not be discussed further in this review.

Chemical Shift-Based Techniques. Chemical shift-based techniques separate the MR signal into its water and fat components by acquiring images at two or more echo times (TEs) after signal excitation. Unlike the fat-suppressed technique, fat suppression (or selective water excitation) pulses are not applied. Two main chemical shift-based approaches are possible: one approach uses magnitude data only (discards phase information) and is referred to here as the magnitude-based approach. The other uses complex data (retains both magnitude and phase information) and is referred to as the complex-based approach. The two approaches are discussed below.

Magnitude-Based Chemical Shift Approach. The magnitude-based approach is probably the most commonly used MR approach for liver fat assessment in current practice. Typically, two gradient echoes are acquired, one at a TE in which the water peak (4.7 ppm) and the dominant fat peak (1.3 ppm) are "out of phase" (or "opposed phase") and one at a TE in which the two peaks are "in phase." Because two echoes are acquired, this is often called "dual-phase" or "dual-echo" imaging. The TEs corresponding to in-phase and out-of-phase (IOP) depend on the field strength. At 1.5T, the chemical shift between water and the dominant fat peak (3.4 ppm) corresponds to a resonance frequency difference of −217 Hz (the main fat peak resonates 217 Hz slower than the water peak). Therefore, at 1.5T signals from water and the main fat peak oscillate with a period of 4.6 msec (=1000 msec / 217 Hz). This means that these signals are in phase every 4.6 msec (ie, 4.6 msec, 9.2 msec, 13.8 msec, etc.) and out of phase at 2.3 msec and every subsequent multiple of 4.6 msec (ie, 2.3 msec 6.9 msec, 11.5 msec). At 3T, the chemical shift corresponds to a frequency difference of −434 Hz. Therefore, the oscillation period at 3T (2.3 msec) is half that at 1.5T (4.6 msec) and the corresponding IP and OP echo times at 3T are halved: water and the main fat peak are in phase every 2.3 msec (ie, 2.3 msec, 4.6 msec, 6.9 msec) and out of phase at 1.15 msec and every subsequent multiple of 2.3 msec (ie, 1.15 msec, 3.45 msec, 5.75 msec). While multiple in-phase and out-of-phase TEs are possible for dual-phase imaging, it is preferable to use the first out-of-phase and the first in-phase TE if possible: ie, 2.3/4.6 msec at 1.5T and 1.15/2.3 msec at 3T, to maximize SNR performance and minimize the effects of T2* decay which worsen as increasing echo times (T2* effects are discussed in greater detail later). Depending on multiple factors (eg, field strength, gradient performance, receiver bandwidth, frequency matrix, slice thickness, fractional echo sampling, scanner software), however, it may not be possible to acquire dual-phase images using the first out-of-phase and in-phase TEs. For example, many early generation 3T scanners do not permit dual-phase imaging with TEs of 1.15 and 2.3 msec; on these scanners, typical TEs for dual-phase imaging are 2.3 and 5.75 msec.

To estimate the signal fat-fraction, we assume 1) the signal intensity from fat is less than the signal intensity from water (ie, $S_{Fat} \leq S_{Water}$); 2) the signal intensity from OP images represents the difference in water and fat signals (ie, $S_{OP} = |S_{Water} - S_{Fat}|$); and 3) the signal intensity from IP images represents the sum of water and fat signals (ie, $S_{IP} = |S_{Water} + S_{Fat}|$) (49).

Rearranging terms in 2) and 3), and assuming 1), the MR signal can be decomposed into its water and

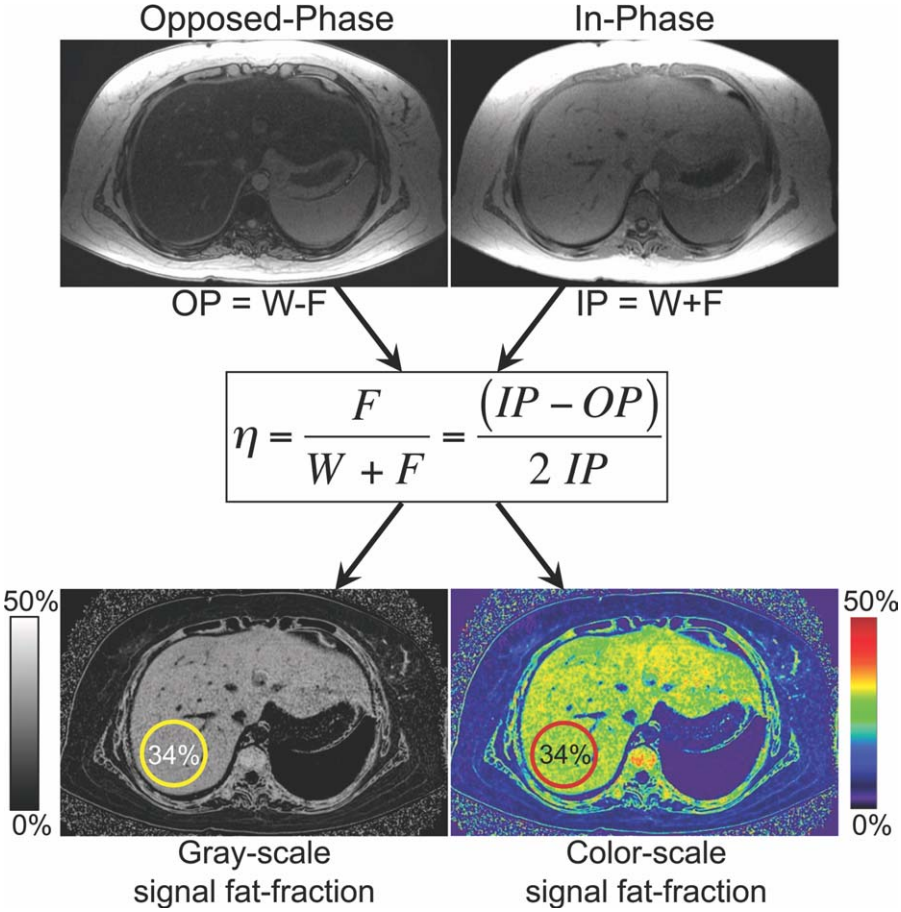

Figure 3. Signal fat-fraction maps can be calculated on a pixel-by-pixel basis using dual-echo (in-phase and opposed phase) imaging using Eq. [3]. Signal fat-fraction maps may not accurately reflect the concentration of fat within the liver unless all confounding factors are addressed. Note that the dynamic range of signal fat-fraction calculated from dual-echo imaging, as well as all magnitude-based methods, is limited to 0%–50%. Fortunately, fat-fractions greater than 50% are uncommon in the liver, although they can occur (eg, Fig. 13). Fat-fraction maps can be displayed in gray-scale or in color.

fat components based on arithmetic combinations of the in-phase and out-of-phase signal intensities:

$$S_{Water} = |S_{IP} + S_{OP}|$$
$$S_{Fat} = |S_{IP} - S_{OP}|$$

Inserting the S_{Fat} and S_{Water} terms into Eq. [1] generates Eq. [3], which permits calculation of the signal fat-fraction from the out-of-phase and in-phase signal intensities:

$$\eta = \frac{|S_{IP} - S_{OP}|}{2^{*}S_{IP}} \qquad [3]$$

This formula can be applied to a region of interest or used on a pixel-by-pixel basis to generate a parametric signal fat-fraction map (Fig. 3). Note, however, that the formula is reliable only for dual-echo sequences in which both echoes (IP and OP) are acquired after the same excitation; the formula may not be valid if the two echoes are acquired separately, as there may be scanner drift or inadvertent changes in calibration setting between acquisitions.

It is important to note that with magnitude-based approaches, it is only possible to achieve a dynamic range of 0-50% signal fat-fraction. This occurs because of a natural ambiguity in assigning fat-water signal dominance with magnitude-only images. As stated above, $S_{OP} = |S_{Water} - S_{Fat}|$. Note that in this equation the S_{OP} is the same if the water and fat signal intensities are swapped. Thus, a tissue in which water signal is dominant will have the same opposed-phase signal intensity as a tissue in which fat signal is dominant. The ramification is that the signal fat-fraction calculated from a single pair of opposed-phase and in-phase echoes cannot distinguish between water-dominant and fat-dominant tissues. For example, a tissue with 30% fat by signal composition would appear to have the same signal fat-fraction as a tissue with 70% fat—both tissues would be assigned a signal fat-fraction of 30%. This phenomenon is apparent on signal fat-fraction maps (Fig. 3), on which subcutaneous adipose tissue (where fat is the dominant signal component) appears darker than fatty liver parenchyma (where water is the dominant signal component). This fat-water signal dominance

ambiguity restricts the dynamic range of magnitude-based chemical shift techniques to 0%–50% signal fat-fraction. Resolving the signal dominance ambiguity problem requires additional information such as complex phase information (50–56), or methods that require acquisition of additional images and exploit differences between water and fat T1 (eg, dual flip angle technique) (57).

Complex-Based Chemical Shift-Based Approach. The complex-based approach (55,58–61) uses both magnitude and phase information from three or more images acquired at echo times appropriate for separation of water and fat signals. Phase shifts result from three main sources: 1) unknown constant, time-independent phase shifts related to coil sensitivities and other system imperfections; 2) known time-dependent phase shifts on fat only resulting from chemical shift differences between water and fat; and 3) unknown time-dependent phase shifts that affect fat and water equally, due to magnetic field inhomogeneities ("field map"). As a result, decomposition methods that use complex data to separate water and fat signals must measure the unknown field map and demodulate (remove) it from the signal. Although including the phase information adds to the complexity to the reconstruction, estimating the field map permits unambiguous water-fat signal separation and allows measurement of the signal fat-fraction over a range of 0%–100%.

Estimation of complex water and fat signals can then be performed using a variety of nonlinear estimation methods such as IDEAL (55,62) or VARPRO (56). The separated water and fat images are coregistered and can be recombined into a signal fat-fraction map as shown in Fig. 4, which permits estimation of the fat-fraction as the fat image divided by the fat and water images.

Unlike the magnitude-based approach, the complex-based approach permits full separation of water and fat signals to achieve a dynamic range of 0%–100% signal fat-fraction, which offers promise as a general solution to fat quantification regardless of the tissue of interest (liver, adipose, bone marrow, etc.). Thus, unlike with the magnitude-based approach, adipose tissue appears bright on signal fat-fraction maps generated by the complex-based approach (Fig. 4).

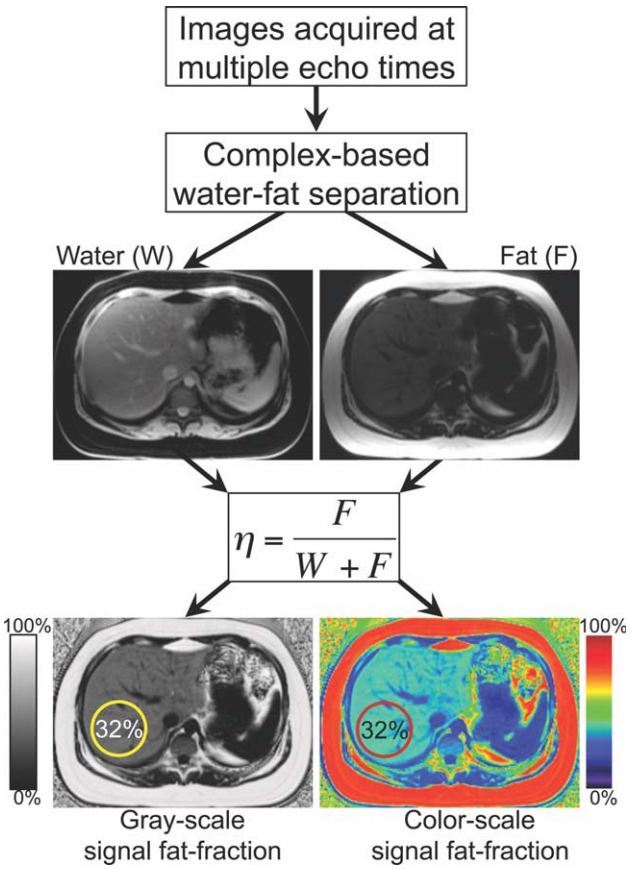

Figure 4. Signal fat-fraction maps with full dynamic range (0%–100%) can be calculated on a pixel-by-pixel basis using Eq. [1], when complex-based fat-water separation methods are used to provide separate fat-only and water-only images. The signal fat-fraction map may not accurately reflect the concentration of fat within the liver unless all confounding factors are addressed. Fat-fraction maps can be displayed in gray-scale or in color.

MR Techniques That Measure the Proton Density Fat-Fraction

As described above, several MR techniques have been developed to measure the signal fat-fraction. These techniques are suitable for depicting the presence and, for the imaging methods, spatial distribution of fat signal from the liver. The signal fat-fraction is confounded by numerous factors, however, and so does not reliably assess fat content. To assess fat content, advanced MRS and MRI techniques have been proposed that address one or more confounding factors (Table 2) (50,55,57–61,63–82). Techniques that address all confounding factors measure proton density fat-fraction. Below, we first describe the confounding factors in general terms and we then discuss more specifically how advanced techniques address these factors.

Factors That Confound the Signal-Fat-Fraction

T1 Bias. T1 bias occurs when images are T1-weighted, resulting in relative amplification of the signal of fat (ie, the shorter T1 proton species), compared to the signal of water (ie, the longer T1 proton species) (Fig. 5). Strategies that avoid T1 weighting or correct for differences in T1 between water and fat reduce T1 bias (59,63). Use of long repetition time for MRS or low flip angle (relative to the repetition time) for chemical shift-based MRI with are commonly used strategies (Fig. 6).

T2 Bias and T2 Decay.* T2 bias is a common confounder for fat quantification methods such as MRS that utilize refocusing pulses to generate echoes. The minimum echo time achievable with clinically available liver MRS sequences is always greater than zero, and therefore some degree of T2 relaxation occurs prior to echo sampling. Because the T2 relaxation time of liver water is shorter than that of liver fat, there is relative amplification of the signal from fat (ie,

Table 2
MRS and MRI Techniques to Quantify Liver Triglycerides

		Confounding factors addressed						
	MR technique	T1	T2/T2*	Fat spectrum	Noise bias	Eddy currents	Resulting method	Literature
MRS	Long TR, Single TE	√	No	No	N/A	N/A	Signal fat-fraction	61, 73, 75, 95
	Long TR, Single TE, fixed T2 correction.	√	Partial	No			Partially T2-corrected signal fat-fraction	96-98
	Long TR, Multiple TE	√	√	No			T2-corrected signal fat-fraction	63, 78, 85, 90, 99
	Long TR, Single TE, fixed T2 correction, Spectrally Corrected	√	Partial	√			Partially T2-corrected signal fat-fraction	14, 100-103
	Long TR Multiple TE, Spectrally Corrected	√	√	√			*Proton density fat-fraction*	82, 84
Magnitude-Based	T1w In/Opposed Phase (IOP) (Conventional MRI)	No	No	No	N/A	N/A	Signal fat-fraction	50, 66-75
	Low-FA IOP	√	No	No			T1-independent Signal fat-fraction	76
	T1w multi-echo	No	√	No			T2*-corrected Signal fat-fraction	79, 104
	Low-FA multi-acquisition IOP	√	√	No			T1-independent, T2*-corrected Signal fat-fraction	57
	Low-FA multi-echo	√	√	No				77
	Low-FA multi-echo with T2* correction and spectral modeling	√	√	√			*Proton density fat-fraction*	63, 78
Complex-based	T1w triple-echo	No	No	No	No	No	Signal fat-fraction	55, 58, 61
	Low-FA triple echo	√	No	No	√	No	T1-independent, noise-bias corrected, signal fat-fraction	59
	Low-FA multi-echo	√	√	No	√	No	T1-independent, T2*-corrected signal fat-fraction	65
	Low-FA triple-echo with spectral modeling	√	No	√	√	No	T1-independent, noise-bias corrected, spectrally modeled signal fat-fraction	81
	Low-FA multi-echo with T2* correction, spectral modeling, and eddy current correction	√	√	√	√	√	*Proton density fat-fraction*	60, 64, 82

Overview of MR spectroscopy and gradient echo-based MRI techniques to assess liver fat. Accurate measurement of proton density fat-fraction with MRS, magnitude-based MRI, or complex-based MRI requires correction for all relevant confounding factors. Note that correction for eddy currents and noise bias are not required for MRS and magnitude-based methods. N/A = not applicable.

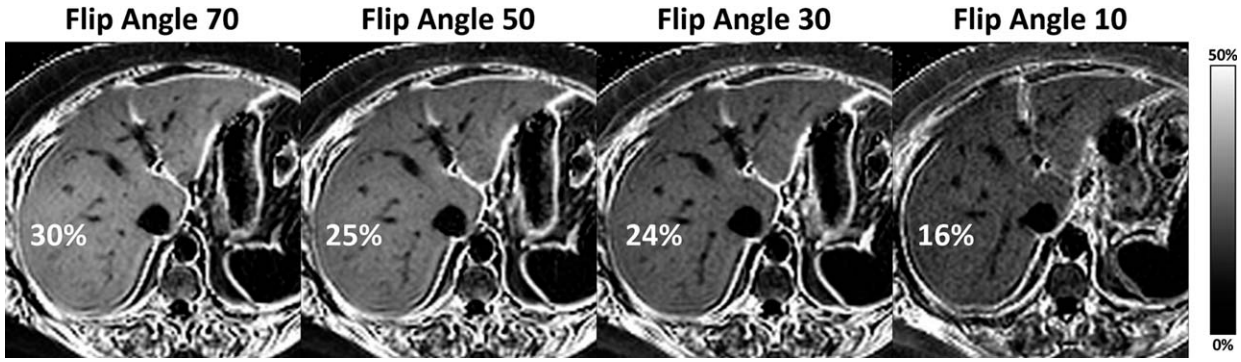

Figure 5. The effect of T1 weighting on fat-fraction estimation is demonstrated in this 39-year-old woman with fatty liver disease. Signal fat-fraction parametric maps were generated from magnitude images at fixed TR (=150 msec) and flip angles of 70, 50, 30, and 10°, and the apparent signal fat-fractions are shown. Reducing T1 weighting by decreasing flip angle can minimize T1 bias, although at a cost of reduced SNR performance. Avoiding T1 bias is important, otherwise the apparent fat-fraction depends on image parameters such as TR and flip angle, and comparisons of results using different protocols or different scanners may be invalid.

the longer T2 proton species) and compared to the signal of water (ie, the shorter T2 proton species). (While it may seem counterintuitive, the T2 of liver fat is longer than T2 of liver water (77,83–85).) One strategy to correct for T2 bias is to use the shortest possible echo time and use population-based water and fat T2 values to correct for T2 decay. This strategy assumes water and fat T2 values are identical across individuals, which may be incorrect and lead to fat quantification errors. To avoid this assumption, an alternative strategy is to collect spectra at multiple echo times, which permits direct measurement of and correction for T2 effects at the individual level.

T2* correction is necessary for chemical shift-based MRI fat-quantification methods that acquire images at increasing echo times after RF excitation. T2* decay leads to increasing signal loss with increasing TE. This confounding effect is amplified by the presence of iron, which commonly coexists with fat in liver disease (86,87). If T2*-related signal decay is not included in the signal model, signal estimation algorithms will incorrectly separate water and fat signals. T2* decay effects are minimized by either incorporating T2* into the signal model used to calculate the fat-fraction, thereby correcting for T2* decay as part of the signal fitting (60,63,65,79), or by measuring T2* separately and correcting for the effects of T2* (57,77,80). Inclusion of T2* into the signal model is advantageous because additional image acquisitions are not required. Yu et al (60,65) and Bydder et al (63) have described T2* correction for complex-based and magnitude-based methods, respectively.

The addition of T2* correction adds additional degrees of freedom (more unknown variables to estimate) to the water-fat separation problem, which has the effect of reducing SNR performance of the method. This can be mitigated in part by increasing the number of echoes in the echo train, which provides better sampling of the signal decay and, hence, more robust estimation of, and correction for, T2* decay. Yu et al have preliminarily demonstrated that at least six echoes are needed for accurate separation of water and fat with T2* correction and complex fitting, although a definitive optimization of the number of echoes

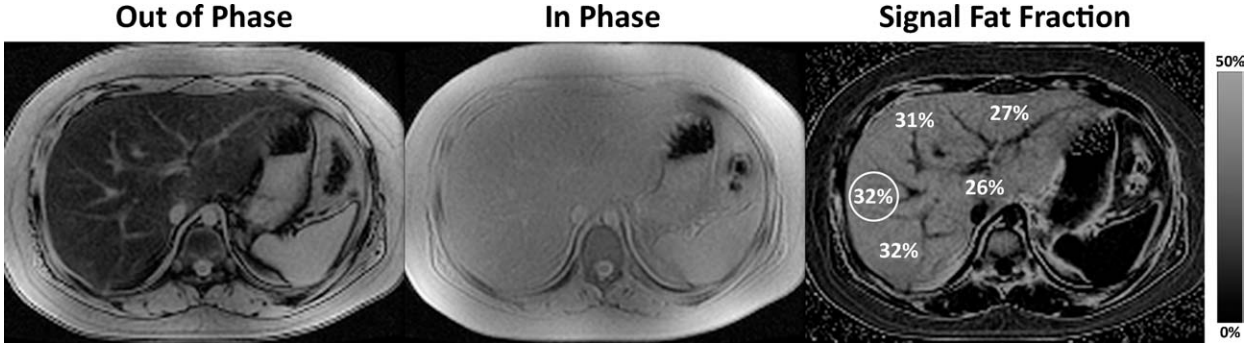

Figure 6. Use of low flip angle is a common strategy to reduce T1 bias using chemical shift methods but does not suffice for accurate PDFF estimation. A 12-year-old boy with fatty liver disease (same subject as in Figs. 11, 12) 2D out-of-phase (TE = 1.15 msec, left) and in-phase (TE = 2.3 msec, center) magnitude gradient echo images were acquired at 3T. To reduce T1 bias, images were acquired with a 10° flip angle and TR of 150 msec. The corresponding signal fat-fraction parametric map (right) was calculated using Eq. [3]. Shown on the map are signal fat-fractions in five regions of interest demonstrating heterogeneity of fat across the liver. The circled region of interest is colocalized to an MRS voxel, where the MRS-determined fat fraction was 39.5%. Thus, while use of low flip angle relative to TR effectively reduces T1 bias, it is not sufficient for accurate fat fraction estimation, as discussed in the text.

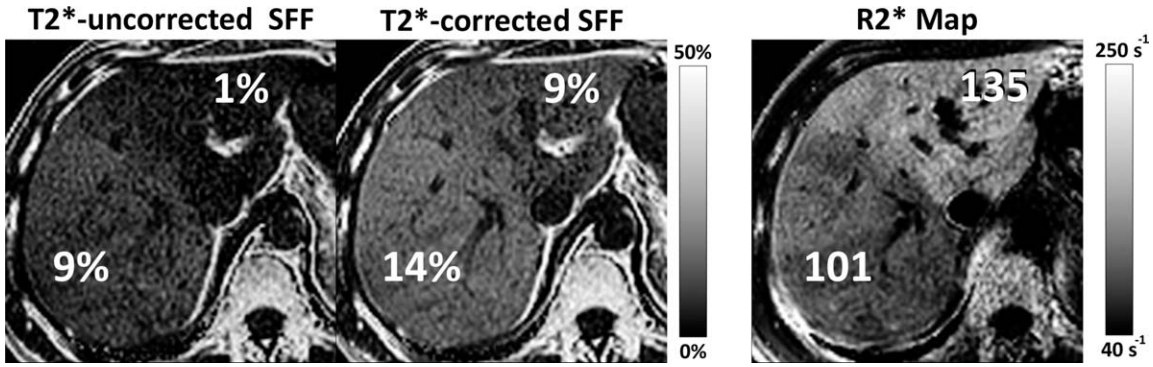

Figure 7. T2* correction is necessary for accurate fat-fraction estimation. A 54-year-old man with concomitant hepatic iron overload and fatty liver. Shown are signal fat-fraction maps generated without T2* correction (left) from a pair of out-of-phase and in-phase magnitude images at 3T (TE = 1.15 and 2.3 msec), and with T2* correction (middle) from nine serial out-of-phase and in-phase images. An R_2* map (=1/T_2*) is generated as part of the T2* correction process (right) (63,65). Compared to the T2*-corrected fat-fraction values, the T2*-uncorrected fat-fraction values are underestimated, particularly in the left lobe. The underestimation of fat-fraction in the left lobe is explained by the R_2* map, because the R_2* in the left lobe of the liver is higher (ie, higher iron concentration).

required for T2* correction for both magnitude and complex fitting methods is still under investigation. Figure 7 shows an example of a magnitude-based fat-water separation method that simultaneously estimates T2*, water and fat. By measuring T2*, any confounding effects of signal decay on echoes acquired at increasing echo time is avoided. For comparison, a magnitude-based fat-water separation method without T2* correction is also shown.

Finally, the assumption that T2* decay is identical for water and fat signals has been challenged. At very low or very high fat-fractions, the "single" T2* model described in Eq. [5] (below) is probably adequate to mitigate the effects of T2*. However, as described by O'Regan et al (79) and Chebrolu et al (88), the use of a "dual" T2* decay model that permits independent correction of water and fat signals may improve accuracy of water-fat separation particularly at high fat-fraction and when T2* is very short (88).

Spectral Complexity of Fat. Fat has a complex chemical spectrum that consists of multiple spectral components. At clinical magnetic field strengths, the spectral components of fat are seen as six distinct spectral peaks at different resonance frequencies (5.3, 4.2, 2.7, 2.1, 1.3, and 0.9 ppm); in liver fat, the relative amplitudes of these peaks are approximately 4.7, 3.9, 0.6, 12.0, 70.0, 8.8%, respectively (Fig. 1, Table 1). These peaks collectively represent the total signal fat-fraction and should all be taken into account for accurate fat quantification. Correction must be made for the fat peaks that do not contribute to the fat signal measurement. If the fat has been measured by the main CH_2 peak (1.3 ppm), the area of the other peaks must be accounted for. If the sum of the visible fat peaks gave the fat fraction, the two peaks (5.3 and 4.2 ppm) that lie close to the water resonance and cannot be differentiated from the water peak by in vivo MRS in fatty liver, must be corrected.

However, there is sufficient information in the four visible peaks to allow spectroscopy to exploit knowledge of the triglyceride chemical structure to determine the type of triglyceride present. This allows calculation of the full fat spectrum and hence the relative fraction of the fat signal that is included in the water peak. The complexity of the fat spectrum is a confounder for imaging techniques that model fat as a single resonance peak (84), eg, the chemical shift-based signal fat-fraction techniques discussed earlier. Ignoring the complexity of the liver fat spectrum results in significant fat quantification errors (78,81), as illustrated in Fig. 8. To correct for the confounding effects of spectral complexity, the MRS-derived full fat spectrum can provide a priori knowledge of the frequency and relative amplitudes of the six fat peaks as shown in Fig. 1 and written explicitly as we show below for the signal models for magnitude- and complex-based techniques. Briefly, the spectral model fits acquired signal data into a mathematical model that correctly takes into account the multipeak interference pattern of fat protons. Detailed description of the model is beyond the scope of this review but can be found in the published literature (55,60,63).

Noise Bias. Noise bias occurs during recombination of separated water and fat images into a fat-fraction image. It is seen in MRI methods that fully separate water and fat signals prior to magnitude reconstruction, such as chemical shift-based water-fat separation methods. Noise bias is particularly marked at low fat-fractions and occurs because areas of low signal (eg, fat signal from a liver or areas with little/no fat) have only positive noise after the magnitude operation. Methods that create fat-fraction maps from in-phase and opposed-phase images (Eq. [2]) are more immune to noise bias except near fat-fractions of 50% when the signal intensity of opposed-phase images approaches zero and noise bias impacts fat-fraction calculations. Noise bias effects are more important in complex-based chemical shift-based water-fat separation methods since low fat-fractions near zero are more clinically relevant. Figure 9 demonstrates the importance of noise related bias and the use of a magnitude discrimination technique to avoid this bias (59).

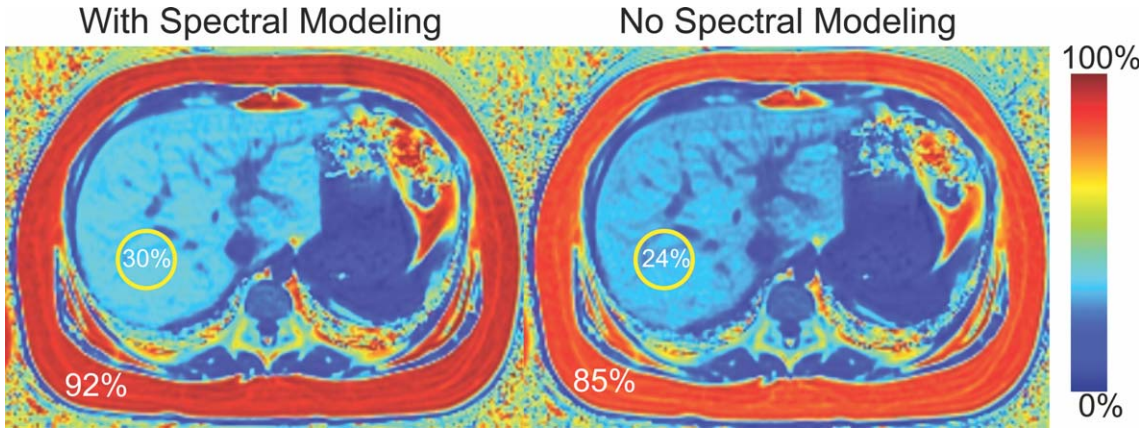

Figure 8. Accurate spectral modeling of fat is necessary to accurately measure liver fat. Complex-based quantitative fat-fraction imaging was performed in a 16-year-old girl with fatty liver, using corrections for all confounding factors, including spectral modeling (left). T2-corrected STEAM MRS (circle) demonstrated 30% fat-fraction by imaging and 29% by MRS, indicating close agreement. The same data were reconstructed using a single-peak model for fat (right), resulting in underestimation of fat-fraction in the liver (24%) and subcutaneous adipose tissue (85%). The fat-fraction in subcutaneous adipose tissue normally ranges between 90%–100%.

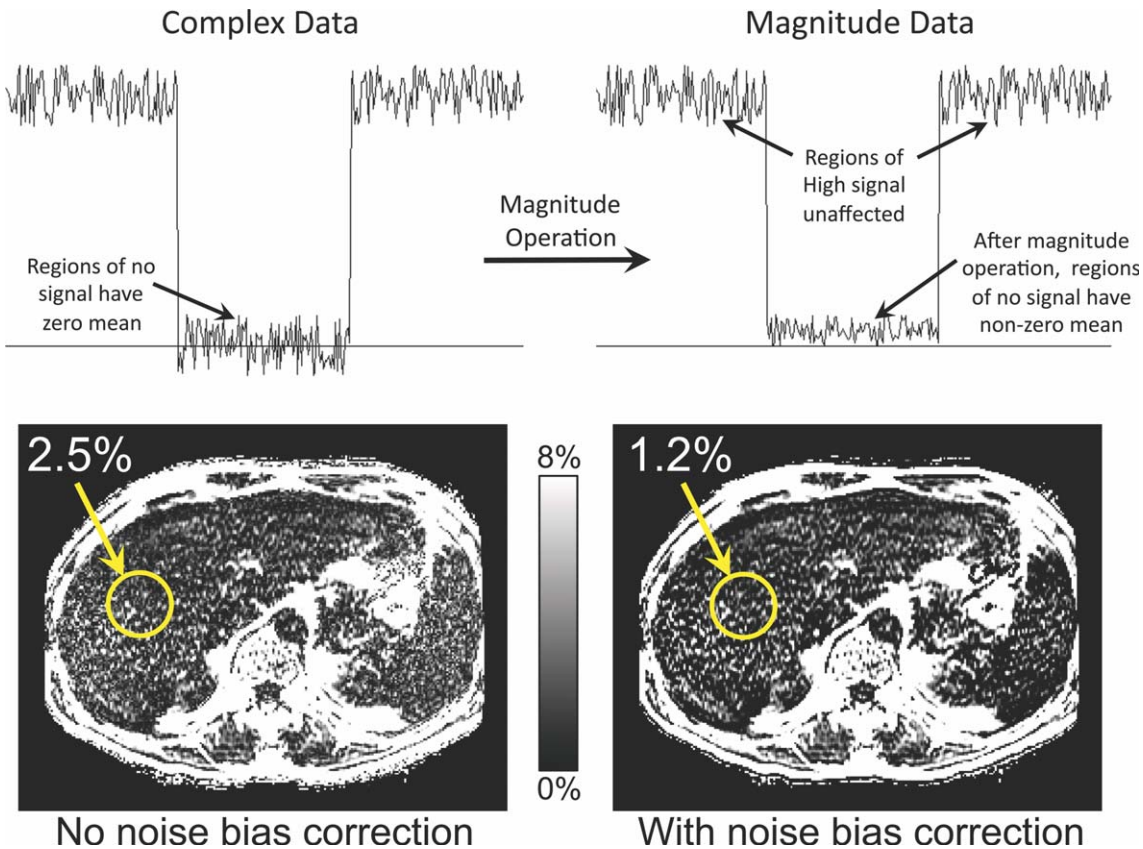

Figure 9. Noise-related bias can result using complex-based MRI techniques when the fat-fraction is close to zero. This occurs because the separated fat and water signals are converted into magnitude images to calculate the fat-fraction. In regions with no fat, the complex fat data has zero mean signal; due to noise, however, about half the pixels in the regions have positive values and about half have negative values (upper left). After the magnitude operation, the negative values are converted into positive values and the mean signal becomes nonzero (upper right). Consequently, the apparent fat-fraction is overestimated (bottom left). Liu et al (59) have described the use of either phase constrained or magnitude discrimination methods (bottom right) to minimize noise-related bias. T2-corrected STEAM MRS demonstrated a true fat-fraction of 1.0%. Images courtesy Diego Hernando, PhD.

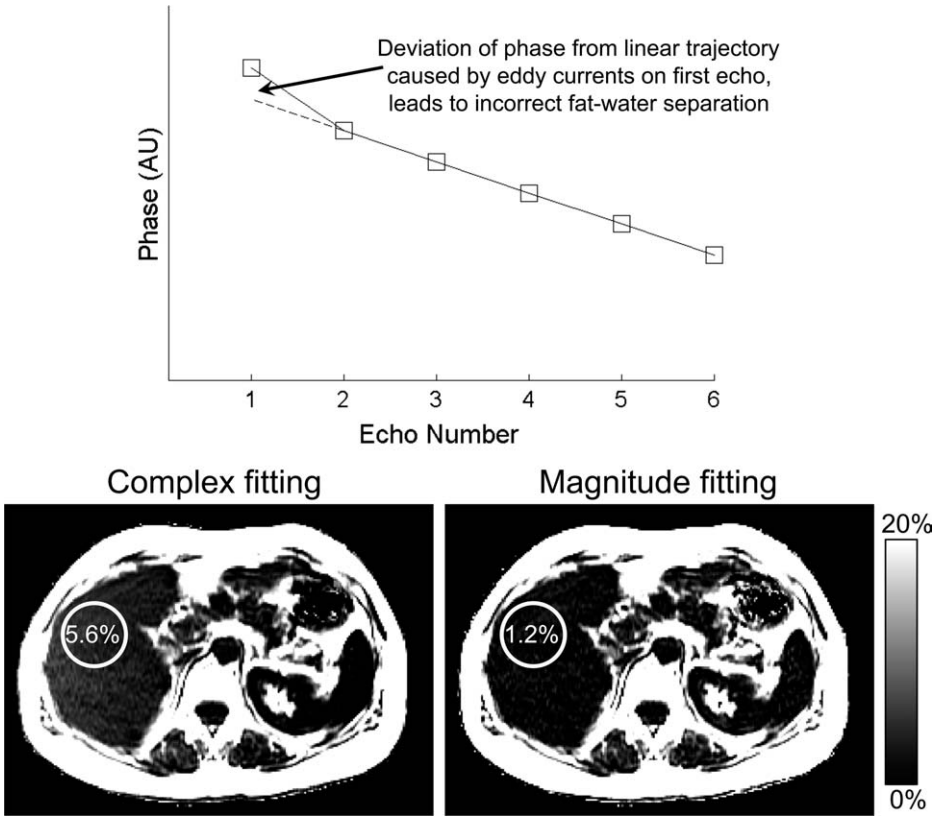

Figure 10. Unexpected phase shifts such as eddy currents can occur echoes acquired at different echo times. In this example, six echoes are acquired in one TR with fly-back gradients between echoes. A schematic diagram (top) demonstrates that the phase of the first echo in a voxel containing only water deviates from a linear trajectory. This deviation in phase leads to overestimation of the fat concentration, because the phase variation mimics signal oscillation from fat-water interference. A hybrid magnitude fitting method applied after complex-based fat-water separation can correct for such errors by discarding phase information (64). In this example, T2-corrected STEAM MRS demonstrated a true fat-fraction of 1.3%, close to the corrected value of 1.2% (right). Images courtesy Diego Hernando, PhD.

Eddy Currents. Eddy currents affect MRI methods that use phase information to quantify fat, such as complex-based chemical shift based water-fat separation methods. Rapid switching of gradients during image acquisition leads to unanticipated phase shifts on images acquired at different echo times, which affects the accuracy of fat-fraction estimates. Importantly, these phase shift are, in general, different at different echo times, leading to incorrect separation of water and fat. The effects of eddy currents are naturally avoided with magnitude-based methods that discard all phase information, including conventional dual echo imaging (50,57,63,66–80). Recently, hybrid approaches that use complex-based separation methods to separate water and fat signals, followed by magnitude-based fitting for "fine-tuning" may be an effective way to achieve fat-fraction measurements with full 0%–100% dynamic range, while minimizing the impact of eddy currents (64). Figure 10 shows an example of the hybrid magnitude fitting approach used with complex-based MRI to avoid meaningful bias. Without this correction, the apparent fat-fraction may lead to incorrect diagnosis of fatty liver disease.

J-Coupling. J-coupling is an intrinsic behavior of all fat peaks (but not the water peak). In both PRESS and STEAM, J-coupled peaks exhibit complex behavior, meaning as TE increases, the observed relaxation of the fat peaks is not well described by T2 decay alone. It is known that not only does J-coupling increase as TE increases, but that PRESS and STEAM differ in their sensitivity to J-coupling. This means that if a large TE range is used to correct for T2 decay, PRESS and STEAM will observe different T2s and give different incorrect estimates of fat-fraction. To minimize the effect of J-coupling, STEAM is chosen as it allows shorter TE than PRESS. However, T2 correction does require measurements at multiple TEs, and hence as short a range of TE as possible should be used to measure T2. The mixing time (TM) in STEAM is also affected by J-coupling and hence the smallest available value of TM should be used.

Most chemical shift based imaging approaches (both magnitude-based and complex-based) for fat quantification are based on low flip angle spoiled gradient echo imaging, and are unaffected by the effects of J-coupling. Quantitative imaging methods that use fast spin-echo approaches, however, may need to consider the effects of J-coupling (89).

Field Strength. Magnetic field strength is a potential confounding factor because T1 and T2* change with field strength, and the chemical shift of fat peaks scales linearly with field strength. Field strength, however, is not expected to influence fat-fraction measurements if low flip angles or long TR are used to avoid T1 bias, and if T2 or T2* correction is performed with spectral modeling.

Below we describe in more detail how advanced MRS and MRI techniques address the confounders to measure the proton density fat-fraction.

Advanced MRS Techniques to Measure Proton Density Fat-Fraction

The spectroscopic measurement of PDDF uses non-water saturated acquisition sequences. To minimize

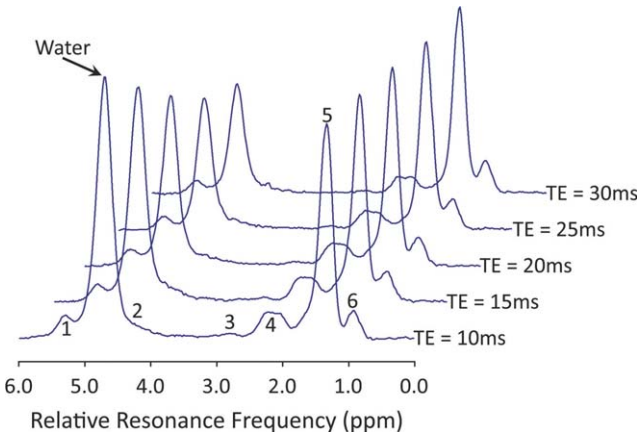

Figure 11. Estimation of PDFF using single-breath-hold T1-independent, T2-corrected, spectrally corrected spectroscopy. A 12-year-old boy with fatty liver disease (same subject as in Figs. 6, 12). After a single preacquisition excitation pulse, five STEAM spectra were acquired at echo times (TEs) of 10, 15, 20, 25, and 30 msec in a single 21-second breath-hold from a single $20 \times 20 \times 20$ mm^3 voxel without averaging at 3T. Notice the water peak decays more rapidly as a function of TE than the main fat peaks, indicating that liver water has shorter T2 than liver fat. TR of 3500 msec and mixing time of 5 msec are used to minimize T1 effects. The MRS voxel is colocalized with the circled region of interest shown in Figs. 6 and 12. Using the nomenclature in Table 1, the water peak and the six resolvable fat peaks are labeled. To estimate the proton density fat-fraction (PDFF), the areas of the water (4.7 ppm) and three major fat spectral peaks (0.9, 1.3, 2.1 ppm) are measured at each TE. For each frequency, the peak area is corrected for T2 decay using nonlinear least-square fitting to determine its relative proton density. The relative proton densities of the two fat peaks (4.2, 5.3 ppm) obscured by the water peak are determined from those of the measurable fat peaks using prior knowledge of the NMR spectrum of liver fat (Table 1) (84), ie, spectrally corrected. The PDFF (39.5% in this case) is then calculated by dividing the fat proton density (sum of all fat peaks) by the sum of the fat and water proton densities. ppm = parts per million.

the effect of J-coupling on the fat peaks, the minimum possible TE is desirable (83). This suggests that STEAM may be preferable to PRESS. To minimize T1 weighting a long TR is used (>3000 msec). Correction for T2 can be performed using a single TE acquisition and predetermined water and fat T2 values, but suffer from poorer accuracy, as they are insensitive to T2 variability of the water peak. Alternatively, recent reports have described rapid, breath-held MR acquisitions with multiple echo times that facilitate measurement of T2 corrected MRS fat-fractions (78,82,90). As there is sufficient SNR even at very low fat-fractions to collect analyzable spectra in a single average, it is feasible to collect multi-TE spectra in a single breath-hold (Fig. 11). A short range of TEs should be used to minimize confounding effects from J-coupling (the authors prefer a TE range of 10–30 msec). A short TE range permits accurate determination of water T2, which is necessary for fat quantification. A short TE range does not permit accurate determination fat T2, but accurate determination of fat T2 is not essential for fat quantification, as fat has significantly longer T2s than water and for a short TE range advocated above, fat-fraction is insensitive to variability in the fat T2.

Advanced MRI Techniques to Measure Proton Density Fat-Fraction

In the following sections the underlying physics of advanced magnitude-based and complex-based quantitative imaging methods is described. Although algorithms that use complex-based imaging are more complicated and involved, the underlying complex-based signal model is more straightforward. Further, the signal model for magnitude-based methods is easily derived from the complex-based signal model. For these reasons, we first describe the complex-based signal method, followed by the magnitude-based method for measuring proton density fat-fraction. Details of these two approaches are described below. Figure 12 shows a comparison of the calculated proton density fat-fraction parametric maps in a patient with severe steatosis using both magnitude-based and complex-based methods.

Complex-Based Chemical Shift Technique. The complex-based chemical shift technique uses both magnitude and phase information from three or more images acquired at echo times appropriate for separation of water and fat signals. In its current implementation, the technique is based on 3D gradient echo imaging. In principle it could be implemented as a 2D sequence but from the published literature this has not been done to our knowledge. To correct for T1 bias, a flip angle of 5° and a repetition time ≥10 msec are typically used at 1.5T. Studies are under way to establish the appropriate flip angle and repetition time appropriate at 3T. As discussed above, a minimum of six echoes are typically used to correct for T2* decay, although studies performed in animal models have been performed comparing 6 and 15 echo acquisitions, demonstrating no difference in estimated fat-fraction (91). As described by Yu et al (65), however, six echoes provide a good balance between short scan time and robust SNR performance of water-fat separation with T2* correction, and also allows relatively flexible echo times with good SNR performance. Thorough optimization of echo times and number of echoes has yet to be performed and may provide important, incremental improvements in fat quantification. The complex-based methods can also correct for spectral complexity of fat, in addition to T2* correction (60). Noise bias is minimized using phase constrained or magnitude discrimination methods developed by Liu et al (59). Eddy current are corrected using the hybrid complex-magnitude approach reported by Yu et al (64). Because the technique is based on complex data (like the water-fat separation technique), it provides estimates of proton density fat-fraction with a dynamic range of 0%–100%. Although a dynamic range of 0%–100% is important for imaging adipose tissue (92) or marrow, it may not be necessary for quantifying hepatic proton density fat-fraction, which seldom exceeds 50%. Currently, the

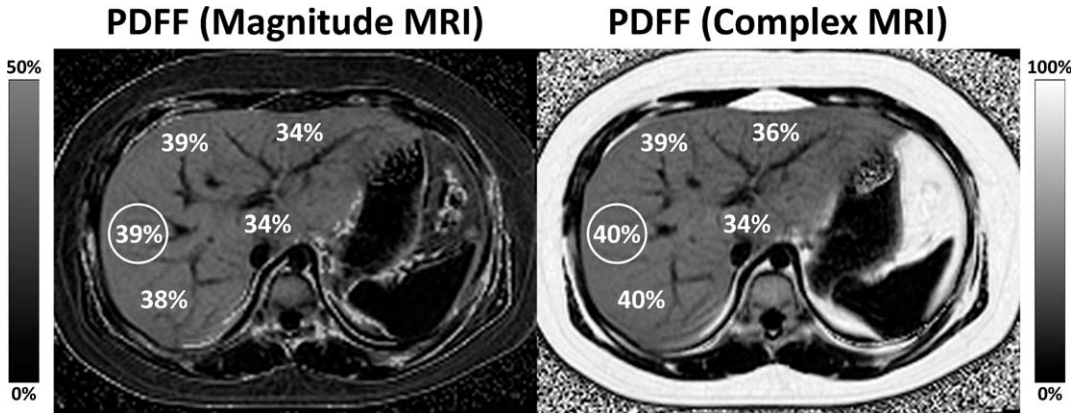

Figure 12. Estimation of PDFF using single-breath-hold T1-independent, T2*-corrected, spectrally modeled magnitude and complex chemical shift-based MRI techniques. A 12-year-old boy with fatty liver disease (same subject as in Figs. 6, 11). Proton density fat-fraction (PDFF) parametric maps were calculated using magnitude (left) and complex (right) chemical shift-based fat-water separation techniques. The magnitude-based technique uses magnitude source images (not shown) to generate a PDFF image with dynamic range of 0%–50%, while the complex-based technique uses complex (magnitude and phase) source images (not shown) to generate a PDFF image with dynamic range of 0%–100%. The two techniques demonstrate excellent agreement both qualitatively and quantitatively for fat within the liver. The two techniques also agree closely with MRS. The calculated PDFF within the circled region of interest is 39% using the magnitude-based technique, 40% using the complex-based technique, and 39.5% using MR spectroscopy (Fig. 10).

technique in its most advanced form is available only as an investigational prototype.

The signal model for the complex signal for a voxel containing water and fat can be written:

$$S(TE) = \left(W + F \sum_{p=1}^{P} r_p e^{i2\pi\Delta f_p TE} \right) e^{i2\pi\psi TE} e^{-TE/T_2^*} \quad [4]$$

where the effects of T2* decay and spectral complexity of fat have been explicitly included, with P distinct spectral peaks of fat resonating at frequency Δf_p and relative amplitude r_p (normalized such that $\sum_{p=1}^{P} r_p = 1$). The complex T2* correction method uses the signal model described in Eq. [5]. A useful feature of this model is that the outer exponential terms of this equation can be combined to form a "complex" field map, ie, $e^{i2\pi\psi TE} e^{-TE/T_2^*} = e^{i2\pi\hat{\psi}TE}$, such that $\hat{\psi} = \psi + \frac{i}{2\pi T_2^*}$. Using this formulation greatly simplifies the estimation of water and fat signals, without adding complexity to the algorithm, while also providing correction for T2*.

Magnitude-Based Chemical Shift Technique. The magnitude-based chemical shift technique discards phase information and uses magnitude images typically acquired at three or more echo times where water and fat signal are in phase and out of phase (50,57,63,66–80). In its current implementation, the technique is based on 2D gradient echo imaging, although it is inherently compatible with 3D imaging. In principle it could be implemented as a 3D sequence but from the published literature this has not been done to our knowledge. To correct for T1 bias, a flip angle of 10° and a repetition time ≥120 msec are typically used at both 1.5T and 3T. T2* decay is corrected by collecting data at six echoes (63), although it is possible that fewer echoes may suffice. The technique also corrects for spectral complexity of fat using the spectral model described above. Noise bias and eddy current effects are considered negligible and do not require correction when using the technique. Because the technique is based on magnitude data (like the dual-echo technique), it cannot accurately quantify proton density fat-fraction beyond the 0%–50% dynamic range and may therefore not suffice for fat-dominant tissues such as adipose tissue or marrow. This limitation may not be clinically important in quantification of hepatic steatosis as the proton density fat-fraction in human liver rarely exceeds 50%.

Magnitude-based methods can be extended to acquisition strategies with more than two echoes, typically six echoes, and are compatible with T2* correction and spectral modeling of fat (63). The basic signal model from a voxel containing a mixture of water and fat is obtained by taking the magnitude of the complex signal model (Eq. [4]), and can be written:

$$|S(TE)| = \sqrt{|W|^2|F|^2 \left| \sum_{p=1}^{P} r_p e^{i2\pi\Delta f_p TE} \right|^2 + 2\mathrm{Re}\left\{ W^* F \sum_{p=1}^{P} r_p e^{i2\pi\Delta f_p TE} \right\}} e^{\frac{-TE}{T_2^*}} \quad [5]$$

where the effects of T2* decay and spectral complexity of fat have been explicitly included (assuming the T2* of water and fat are equal), with P distinct spectral peaks of fat resonating at frequency Δf_p and relative amplitude r_p (normalized such that $\sum_{p=1}^{P} r_p = 1$), the vertical bars denote absolute value (ie, magnitude values of water and fat), Re{ } denotes the real part of the quantity, and the asterisk denotes complex conjugate. Nonlinear signal estimation methods can then be used to estimate the amount of fat and water, to determine the proton density fat-fraction (63,64,79).

Performance and Utility of MRI Techniques That Measure the Proton Density Fat-Fraction. The complex- and magnitude-based chemical shift techniques have

demonstrated excellent correlation and agreement with known proton density fat-fractions in phantom experiments (63,93), animal experiments (94) and in clinical studies that compare them to single voxel MRS (78,82). In a clinical study on 110 patients imaged at 1.5T using the magnitude-based chemical shift technique, excellent correlation with MRS was demonstrated with a slope = 0.98 CI = [0.92, 1.04], and intercept = 0.91% CI = [−0.18%, 1.99%] (78). Excellent correlation has also been observed using the complex-based chemical shift technique at 1.5T on 54 patients, with $r^2 = 0.99$, slope = 1.00 ± 0.01%, and intercept = 0.2 ± 0.1%) (82). More recently, a large cohort study at 3T has shown similar results for the magnitude-based method (95).

Although the exact threshold between normal and abnormal liver fat is not fully understood, a commonly used fat-fraction threshold of 5.56% is commonly used. This threshold is based on a large MR spectroscopy study performed in 2349 participants of the Dallas Heart Study (14), in which the 95th percentile cutoff of 5.56% fat-fraction was determined from a subset of 345 patients with no identifiable risk factors for steatosis. Using this threshold, both complex- and magnitude-based chemical shift techniques have accuracies close to 100% for the detection of steatosis (78,82), and can potentially be used to classify patients as having clinically significant steatosis.

Currently, the multiecho magnitude based pulse sequence described by Bydder et al (63) can be reproduced easily using standard, available pulse sequences, although the reconstruction of fat-fraction images is only available at limited sites. Complex-based methods such as those described by Yu et al (60) are only available as investigational pulse sequences and reconstruction methods. Such methods and may be available commercially in the near future.

Because they are quantitative and accurate when performed properly, both magnitude-based and complex-based methods have a role in longitudinal monitoring of liver fat. For example, Fig. 13 shows the impact of plasmapheresis in a patient with severe hypertriglyceridemia and the associated fatty liver disease. Please also note that that proton density fat-fraction exceeded 50% in this extreme case. Such methods can also be used to characterize the concentration of fat within fat-containing lesions such as HCC or adenoma (Fig. 14). This is an emerging utility of fat quantification methods, but the clinical significance of this application is unclear and research in this area is necessary. Further, the relevance of fat quantification methods in liver will likely extend to other clinical specialties, including endocrinology, where diseases such as polycystic ovary syndrome (PCOS) are associated with metabolic abnormalities, including insulin resistance and fatty liver disease (Fig. 15).

CONCLUSION

In summary, while liver biopsy is the current reference standard for assessment of hepatic steatosis, it has several drawbacks that make it a suboptimal tool

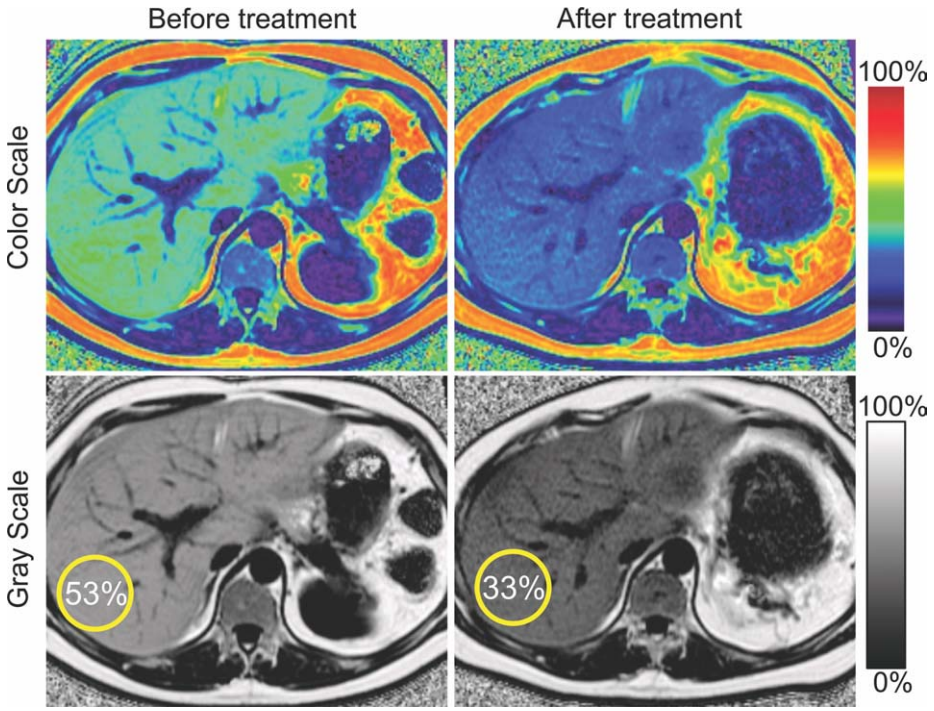

Figure 13. Serial liver MRI exams can be used to demonstrate changes in liver fat during therapy. Serial PDFF maps obtained with complex-based MRI were acquired in a 41-year-old man with hypertriglyceridemia and insulin resistance undergoing plasmapheresis and multidrug therapy to lower serum triglycerides. Follow-up MRI demonstrates reduction in hepatic PDFF (from 53% to 33%). Notice the corresponding reduction in liver size. This example demonstrates that fat-fractions greater than 50% may occur, and it also illustrates the use of gray-scale and color-scale PDFF maps.

Figure 14. Quantitative MRI can be used to assess the concentration of fat in fat-containing liver masses such as hepatic adenomas. The estimated proton density fat-fraction is 19% in this pathology-proven lipid rich adenoma. Conventional T1-weighted dual-echo images are shown for comparison; notice signal loss on the opposed-phase image. Quantifying fat in such lesions currently has unclear clinical utility but potentially may offer insight into pathophysiology.

for establishing the diagnosis and severity of steatosis, as well as longitudinal follow-up of patients with liver fat. Noninvasive methods to assess liver fat are needed. Of available imaging modalities, MR-based techniques measure liver fat most directly and, if performed correctly, accurately. A key concept that was discussed in this article is that the MR-determined signal fat-fraction is a confounded measurement of liver fat content that, in general, depends on the platform and specific scan parameters. For these reasons, signal fat-fraction is not a consistently useful or broadly applicable biomarker of hepatic steatosis. By comparison, the proton density fat-fraction is an inherent physical property of tissue that provides an unconfounded measurement of liver fat content and, based both on theory and experimental studies, is

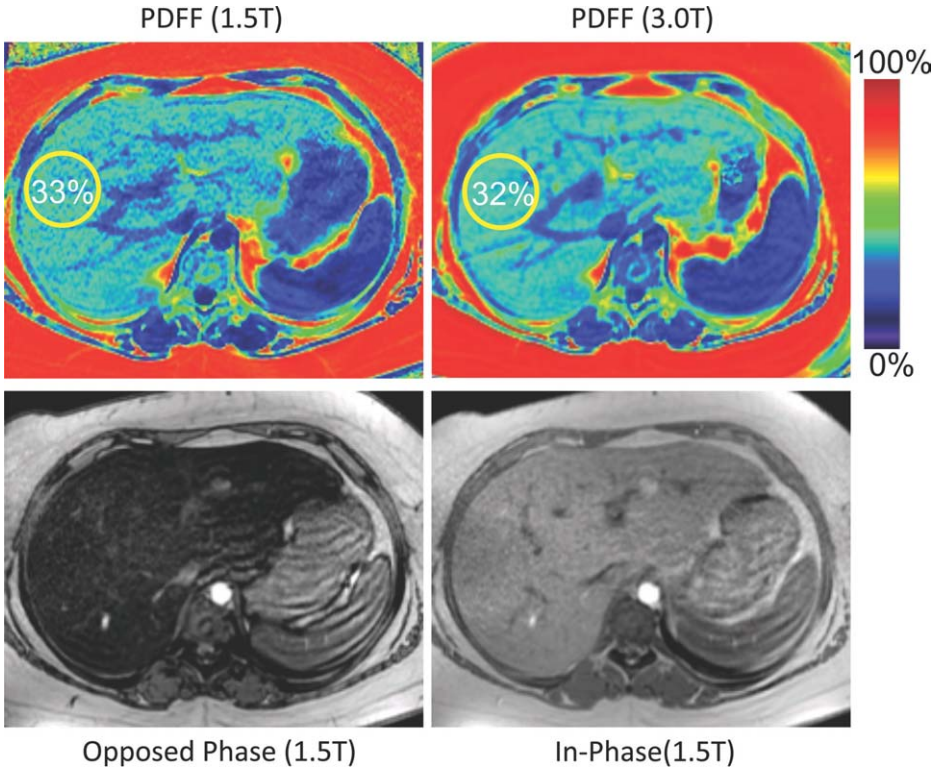

Figure 15. Quantitative proton density fat-fraction imaging performed in a 16-year-old girl with polycystic ovary syndrome (PCOS) demonstrates severe steatosis. PCOS is a condition associated with insulin resistance and NAFLD. Quantitative fat-fraction imaging in PCOS may be an emerging application in an adolescent population that is often reticent undergo to liver biopsy. In this patient, aminotransferases were mildly elevated, raising concern for steatohepatitis. Biopsy demonstrated severe steatohepatitis. Complex-based PDFF maps acquired at 1.5T (PDFF = 33%) and 10 days later at 3T (PDFF = 32%) demonstrate close qualitative and quantitative agreement. Conventional T1-weighted dual-echo images (1.5T) demonstrating marked signal drop-out on opposed phase imaging are shown for comparison.

emerging as a valid biomarker of liver fat content. Advanced MRI techniques currently under development have demonstrated high potential for accurate detection and quantification of hepatic steatosis using proton density fat-fraction. Given the excellent agreement of the imaging methods with MRS, the quantitative imaging approaches to fat quantification are generally preferable to MRS as they provide spatial coverage of the liver. However, further technical refinement and validation is still required for the techniques to be universally accepted as biomarkers of hepatic fat accumulation.

REFERENCES

1. Adams LA, Lymp JF, St Sauver J, et al. The natural history of nonalcoholic fatty liver disease: a population-based cohort study. Gastroenterology 2005;129:113–121.
2. Adams LA, Waters OR, Knuiman MW, Elliott RR, Olynyk JK. NAFLD as a risk factor for the development of diabetes and the metabolic syndrome: an eleven-year follow-up study. Am J Gastroenterol 2009;104:861–867.
3. Dunn W, Xu R, Wingard DL, et al. Suspected nonalcoholic fatty liver disease and mortality risk in a population-based cohort study. Am J Gastroenterol 2008;103:2263–2271.
4. Fabbrini E, deHaseth D, Deivanayagam S, Mohammed BS, Vitola BE, Klein S. Alterations in fatty acid kinetics in obese adolescents with increased intrahepatic triglyceride content. Obesity (Silver Spring) 2009;17:25–29.
5. Korenblat KM, Fabbrini E, Mohammed BS, Klein S. Liver, muscle, and adipose tissue insulin action is directly related to intrahepatic triglyceride content in obese subjects. Gastroenterology 2008;134:1369–1375.
6. Lok AS, Everhart JE, Chung RT, et al. Evolution of hepatic steatosis in patients with advanced hepatitis C: results from the hepatitis C antiviral long-term treatment against cirrhosis (HALT-C) trial. Hepatology 2009;49:1828–1837.
7. Lok AS, Everhart JE, Chung RT, et al. Hepatic steatosis in hepatitis C: comparison of diabetic and nondiabetic patients in the hepatitis C antiviral long-term treatment against cirrhosis trial. Clin Gastroenterol Hepatol 2007;5:245–254.
8. Matteoni CA, Younossi ZM, Gramlich T, Boparai N, Liu YC, McCullough AJ. Nonalcoholic fatty liver disease: a spectrum of clinical and pathological severity. Gastroenterology 1999;116: 1413–1419.
9. Rubinstein E, Lavine JE, Schwimmer JB. Hepatic, cardiovascular, and endocrine outcomes of the histological subphenotypes of nonalcoholic fatty liver disease. Semin Liver Dis 2008;28: 380–385.
10. Sanyal AJ, Banas C, Sargeant C, et al. Similarities and differences in outcomes of cirrhosis due to nonalcoholic steatohepatitis and hepatitis C. Hepatology 2006;43:682–689.
11. Ekstedt M, Franzen LE, Mathiesen UL, et al. Long-term follow-up of patients with NAFLD and elevated liver enzymes. Hepatology 2006;44:865–873.
12. Clark JM, Diehl AM. Defining nonalcoholic fatty liver disease: implications for epidemiologic studies. Gastroenterology 2003; 124:248–250.
13. Ioannou GN. Development and validation of a model predicting graft survival after liver transplantation. Liver Transpl 2006;12: 1594–1606.
14. Szczepaniak LS, Nurenberg P, Leonard D, et al. Magnetic resonance spectroscopy to measure hepatic triglyceride content: prevalence of hepatic steatosis in the general population. Am J Physiol Endocrinol Metab 2005;288:E462–468.
15. Ludwig J, Viggiano T, DB M, Oh B. Nonalcoholic steatohepatitis: Mayo Clinic experience with a hitherto unnamed disease. Mayo Clin Proc 1980;55:434–438.
16. Angulo P, Keach JC, Batts KP, Lindor KD. Independent predictors of liver fibrosis in patients with nonalcoholic steatohepatitis. Hepatology 1999;30:1356–1362.
17. Gramlich T, Kleiner DE, McCullough AJ, Matteoni CA, Boparai N, Younossi ZM. Pathologic features associated with fibrosis in nonalcoholic fatty liver disease. Hum Pathol 2004;35:196–199.
18. Guzman G, Brunt EM, Petrovic LM, Chejfec G, Layden TJ, Cotler SJ. Does nonalcoholic fatty liver disease predispose patients to hepatocellular carcinoma in the absence of cirrhosis? Arch Pathol Lab Med 2008;132:1761–1766.
19. Schindhelm RK, Diamant M, Heine RJ. Nonalcoholic fatty liver disease and cardiovascular disease risk. Curr Diab Rep 2007;7: 181–187.
20. Targher G, Arcaro G. Non-alcoholic fatty liver disease and increased risk of cardiovascular disease. Atherosclerosis 2007; 191:235–240.
21. Angelico M. Donor liver steatosis and graft selection for liver transplantation: a short review. Eur Rev Med Pharmacol Sci 2005;9:295–297.
22. Ploeg RJ, D'Alessandro AM, Knechtle SJ, et al. Risk factors for primary dysfunction after liver transplantation—a multivariate analysis. Transplantation 1993;55:807–813.
23. Yoong KF, Gunson BK, Neil DA, et al. Impact of donor liver microvesicular steatosis on the outcome of liver retransplantation. Transplant Proc 1999;31:550–551.
24. Busuttil RW, Tanaka K. The utility of marginal donors in liver transplantation. Liver Transpl 2003;9:651–663.
25. Brunt EM, Janney CG, Di Bisceglie AM, Neuschwander-Tetri BA, Bacon BR. Nonalcoholic steatohepatitis: a proposal for grading and staging the histological lesions. Am J Gastroenterol 1999;94: 2467–2474.
26. Marsman H, Matsushita T, Dierkhising R, et al. Assessment of donor liver steatosis: pathologist or automated software? Hum Pathol 2004;35:430–435.
27. Zaitoun AM, Al Mardini H, Awad S, Ukabam S, Makadisi S, Record CO. Quantitative assessment of fibrosis and steatosis in liver biopsies from patients with chronic hepatitis C. J Clin Pathol 2001;54:461–465.
28. Bravo A, Sheth S, Chopra S. Liver biopsy. N Engl J Med 2001; 344:495–500.
29. Ratziu V, Charlotte F, Heurtier A, et al. Sampling variability of liver biopsy in nonalcoholic fatty liver disease. Gastroenterology 2005;128:1898–1906.
30. Emond MJ, Bronner MP, Carlson TH, Lin M, Labbe RF, Kowdley KV. Quantitative study of the variability of hepatic iron concentrations. Clin Chem 1999;45:340–346.
31. Villeneuve JP, Bilodeau M, Lepage R, Cote J, Lefebvre M. Variability in hepatic iron concentration measurement from needle-biopsy specimens. J Hepatol 1996;25:172–177.
32. Abdi W, Millan JC, Mezey E. Sampling variability on percutaneous liver biopsy. Arch Intern Med 1979;139:667–669.
33. Baunsgaard P, Sanchez GC, Lundborg CJ. The variation of pathological changes in the liver evaluated by double biopsies. Acta Pathol Microbiol Scand [A] 1979;87:51–57.
34. Bedossa P, Dargere D, Paradis V. Sampling variability of liver fibrosis in chronic hepatitis C. Hepatology 2003;38:1449–1457.
35. Labayle D, Chaput JC, Albuisson F, Buffet C, Martin E, Etienne JP. [Comparison of the histological lesions in tissue specimens taken from the right and left lobe of the liver in alcoholic liver disease (author's transl).] Gastroenterol Clin Biol 1979; 3:235–240.
36. Maharaj B, Maharaj RJ, Leary WP, et al. Sampling variability and its influence on the diagnostic yield of percutaneous needle biopsy of the liver. Lancet 1986;1:523–525.
37. Olsson R, Hagerstrand I, Broome U, et al. Sampling variability of percutaneous liver biopsy in primary sclerosing cholangitis. J Clin Pathol 1995;48:933–935.
38. Regev A, Berho M, Jeffers LJ, et al. Sampling error and intraobserver variation in liver biopsy in patients with chronic HCV infection. Am J Gastroenterol 2002;97:2614–2618.
39. Charatcharoenwitthaya P, Lindor KD. Role of radiologic modalities in the management of non-alcoholic steatohepatitis. Clin Liver Dis 2007;11:37–54, viii.
40. Mishra P, Younossi ZM. Abdominal ultrasound for diagnosis of nonalcoholic fatty liver disease (NAFLD). Am J Gastroenterol 2007;102:2716–2717.
41. Saadeh S, Younossi ZM, Remer EM, et al. The utility of radiological imaging in nonalcoholic fatty liver disease. Gastroenterology 2002;123:745–750.
42. Mottin CC, Moretto M, Padoin AV, et al. The role of ultrasound in the diagnosis of hepatic steatosis in morbidly obese patients. Obes Surg 2004;14:635–637.

43. Graif M, Yanuka M, Baraz M, et al. Quantitative estimation of attenuation in ultrasound video images: correlation with histology in diffuse liver disease. Invest Radiol 2000;35:319–324.
44. Kodama Y, Ng CS, Wu TT, et al. Comparison of CT methods for determining the fat content of the liver. AJR Am J Roentgenol 2007;188:1307–1312.
45. Lee SW, Park SH, Kim KW, et al. Unenhanced CT for assessment of macrovesicular hepatic steatosis in living liver donors: comparison of visual grading with liver attenuation index. Radiology 2007;244:479–485.
46. Limanond P, Raman SS, Lassman C, et al. Macrovesicular hepatic steatosis in living related liver donors: correlation between CT and histologic findings. Radiology 2004;230: 276–280.
47. Fazel R, Krumholz HM, Wang Y, et al. Exposure to low-dose ionizing radiation from medical imaging procedures. N Engl J Med 2009;361:849–857.
48. Birnbaum BA, Hindman N, Lee J, Babb JS. Multi-detector row CT attenuation measurements: assessment of intra- and interscanner variability with an anthropomorphic body CT phantom. Radiology 2007;242:109–119.
49. Dixon WT. Simple proton spectroscopic imaging. Radiology 1984; 153:189–194.
50. Qayyum A, Goh JS, Kakar S, Yeh BM, Merriman RB, Coakley FV. Accuracy of liver fat quantification at MR imaging: comparison of out-of-phase gradient-echo and fat-saturated fast spin-echo techniques—initial experience. Radiology 2005;237:507–511.
51. Glover GH, Schneider E. Three-point Dixon technique for true water/fat decomposition with B0 inhomogeneity correction. Magn Reson Med 1991;18:371–383.
52. Xiang Q, An L. Water-fat imaging with direct phase encoding. J Magn Reson Imaging 1997;7:1002–1015.
53. Ma J. Breath-hold water and fat imaging using a dual-echo two-point Dixon technique with an efficient and robust phase-correction algorithm. Magn Reson Med 2004;52:415–419.
54. Reeder SB, Pineda AR, Wen Z, et al. Iterative decomposition of water and fat with echo asymmetry and least-squares estimation (IDEAL): application with fast spin-echo imaging. Magn Reson Med 2005;54:636–644.
55. Reeder SB, McKenzie CA, Pineda AR, et al. Water-fat separation with IDEAL gradient-echo imaging. J Magn Reson Imaging 2007; 25:644–652.
56. Hernando D, Haldar JP, Sutton BP, Ma J, Kellman P, Liang ZP. Joint estimation of water/fat images and field inhomogeneity map. Magn Reson Med 2008;59:571–580.
57. Hussain HK, Chenevert TL, Londy FJ, et al. Hepatic fat fraction: MR imaging for quantitative measurement and display—early experience. Radiology 2005;237:1048–1055.
58. Kovanlikaya A, Guclu C, Desai C, Becerra R, Gilsanz V. Fat quantification using three-point Dixon technique: in vitro validation. Acad Radiol 2005;12:636–639.
59. Liu CY, McKenzie CA, Yu H, Brittain JH, Reeder SB. Fat quantification with IDEAL gradient echo imaging: correction of bias from T (1) and noise. Magn Reson Med 2007;58:354–364.
60. Yu H, Shimakawa A, McKenzie CA, Brodsky E, Brittain JH, Reeder SB. Multiecho water-fat separation and simultaneous R2* estimation with multifrequency fat spectrum modeling. Magn Reson Med 2008;60:1122–1134.
61. Kim H, Taksali SE, Dufour S, et al. Comparative MR study of hepatic fat quantification using single-voxel proton spectroscopy, two-point Dixon and three-point IDEAL. Magn Reson Med 2008; 59:521–527.
62. Reeder SB, Wen Z, Yu H, et al. Multicoil Dixon chemical species separation with an iterative least-squares estimation method. Magn Reson Med 2004;51:35–45.
63. Bydder M, Yokoo T, Hamilton G, et al. Relaxation effects in the quantification of fat using gradient echo imaging. Magn Reson Imaging 2008;26:347–359.
64. Yu H, Shimakawa A, Hines CD, McKenzie CA, Hamilton G, Sirlin CB, Brittain JH, Reeder SB. Combination of complex-based and magnitude-based multiecho water-fat separation for accurate quantification of fat-fraction. Magn Reson Med 2011;66:199–206.
65. Yu H, McKenzie CA, Shimakawa A, et al. Multiecho reconstruction for simultaneous water-fat decomposition and T2* estimation. J Magn Reson Imaging 2007;26:1153–1161.
66. Mitchell DG, Kim I, Chang TS, et al. Fatty liver. Chemical shift phase-difference and suppression magnetic resonance imaging techniques in animals, phantoms, and humans. Invest Radiol 1991;26:1041–1052.
67. Levenson H, Greensite F, Hoefs J, et al. Fatty infiltration of the liver: quantification with phase-contrast MR imaging at 1.5 T vs biopsy. AJR Am J Roentgenol 1991;156:307–312.
68. Kawamitsu H, Kaji Y, Ohara T, Sugimura K. Feasibility of quantitative intrahepatic lipid imaging applied to the magnetic resonance dual gradient echo sequence. Magn Reson Med Sci 2003;2: 47–50.
69. Rinella ME, McCarthy R, Thakrar K, et al. Dual-echo, chemical shift gradient-echo magnetic resonance imaging to quantify hepatic steatosis: implications for living liver donation. Liver Transpl 2003;9:851–856.
70. Pacifico L, Celestre M, Anania C, Paolantonio P, Chiesa C, Laghi A. MRI and ultrasound for hepatic fat quantification: relationships to clinical and metabolic characteristics of pediatric nonalcoholic fatty liver disease. Acta Paediatr 2007;96: 542–547.
71. Schuchmann S, Weigel C, Albrecht L, et al. Non-invasive quantification of hepatic fat fraction by fast 1.0, 1.5 and 3.0 T MR imaging. Eur J Radiol 2007;62:416–422.
72. Yoshimitsu K, Kuroda Y, Nakamuta M, et al. Noninvasive estimation of hepatic steatosis using plain CT vs. chemical-shift MR imaging: significance for living donors. J Magn Reson Imaging 2008;28:678–684.
73. Cowin GJ, Jonsson JR, Bauer JD, et al. Magnetic resonance imaging and spectroscopy for monitoring liver steatosis. J Magn Reson Imaging 2008;28:937–945.
74. Borra RJ, Salo S, Dean K, et al. Nonalcoholic fatty liver disease: rapid evaluation of liver fat content with in-phase and out-of-phase MR imaging. Radiology 2009;250:130–136.
75. McPherson S, Jonsson JR, Cowin GJ, et al. Magnetic resonance imaging and spectroscopy accurately estimate the severity of steatosis provided the stage of fibrosis is considered. J Hepatol 2009;51:389–397.
76. Fishbein MH, Gardner KG, Potter CJ, Schmalbrock P, Smith MA. Introduction of fast MR imaging in the assessment of hepatic steatosis. Magn Reson Imaging 1997;15:287–293.
77. Guiu B, Petit JM, Loffroy R, et al. Quantification of liver fat content: comparison of triple-echo chemical shift gradient-echo imaging and in vivo proton MR spectroscopy. Radiology 2009; 250:95–102.
78. Yokoo T, Bydder M, Hamilton G, et al. Nonalcoholic fatty liver disease: diagnostic and fat-grading accuracy of low-flip-angle multiecho gradient-recalled-echo MR imaging at 1.5 T. Radiology 2009;251:67–76.
79. O'Regan DP, Callaghan MF, Wylezinska-Arridge M, et al. Liver fat content and T2*: simultaneous measurement by using breath-hold multiecho MR imaging at 3.0 T—feasibility. Radiology 2008; 247:550–557.
80. d'Assignies G, Ruel M, Khiat A, et al. Noninvasive quantitation of human liver steatosis using magnetic resonance and bioassay methods. Eur Radiol 2009;19:2033–2040.
81. Reeder SB, Robson PM, Yu H, et al. Quantification of hepatic steatosis with MRI: the effects of accurate fat spectral modeling. J Magn Reson Imaging 2009;29:1332–1339.
82. Meisamy S, Hines C, Hamilton G, et al. Quantification of hepatic steatosis using T1 independent, T2* corrected MRI with spectral modeling of fat: a blinded comparison with MR spectroscopy. Radiology 2011;258:767–775.
83. Hamilton G, Middleton MS, Bydder M, et al. Effect of PRESS and STEAM sequences on magnetic resonance spectroscopic liver fat quantification. J Magn Reson Imaging 2009;30:145–152.
84. Hamilton G, Yokoo T, Bydder M, et al. In vivo characterization of the liver fat (1)H MR spectrum. NMR Biomed 2010 [Epub ahead of print].
85. Thomsen C, Becker U, Winkler K, Christoffersen P, Jensen M, Henriksen O. Quantification of liver fat using magnetic resonance spectroscopy. Magn Reson Imaging 1994;12:487–495.
86. Bonkovsky HL, Jawaid Q, Tortorelli K, et al. Non-alcoholic steatohepatitis and iron: increased prevalence of mutations of the HFE gene in non-alcoholic steatohepatitis. J Hepatol 1999;31: 421–429.

87. George DK, Goldwurm S, MacDonald GA, et al. Increased hepatic iron concentration in nonalcoholic steatohepatitis is associated with increased fibrosis. Gastroenterology 1998;114: 311–318.
88. Chebrolu VV, Hines CD, Yu H, et al. Independent estimation of T*2 for water and fat for improved accuracy of fat quantification. Magn Reson Med 2010;63:849–857.
89. Li Z, Graff C, Gmitro AF, et al. Rapid water and lipid imaging with T2 mapping using a radial IDEAL-GRASE technique. Magn Reson Med 2009;61:1415–1424.
90. Pineda N, Sharma P, Xu Q, Hu X, Vos M, Martin DR. Measurement of hepatic lipid: high-speed T2-corrected multiecho acquisition at 1H MR spectroscopy—a rapid and accurate technique. Radiology 2009;252:568–576.
91. Hines CD, Yu H, Shimakawa A, McKenzie CA, Warner TF, Brittain JH, Reeder SB. Quantification of hepatic steatosis with 3-T MR imaging: validation in ob/ob mice. Radiology 2010;254: 119–128.
92. Bornert P, Keupp J, Eggers H, Aldefeld B. Whole-body 3D water/fat resolved continuously moving table imaging. J Magn Reson Imaging 2007;25:660–665.
93. Hines CD, Yu H, Shimakawa A, McKenzie CA, Brittain JH, Reeder SB. T1 independent, T2* corrected MRI with accurate spectral modeling for quantification of fat: validation in a fat-water-SPIO phantom. J Magn Reson Imaging 2009;30:1215–1222.
94. Hines CD, Yu H, Shimakawa A, et al. Quantification of hepatic steatosis with 3-T MR imaging: validation in ob/ob mice. Radiology 2010;254:119–128.
95. Yokoo T, Shiehmorteza M, Bydder M, et al. Spectrally-modeled hepatic fat quantification by multi-echo gradient-recalled-echo magnetic resonance imaging at 3.0T. In: Proc 17th Annual Meeting ISMRM, Honolulu; 2009.